NASA Contractor Report 3924

A Theoretical Study of Non-Adiabatic Surface Effects for a Model in the NTF Cryogenic Wind Tunnel

J. M. Macha, L. A. Pare,
and D. B. Landrum

GRANT NAG1-417
AUGUST 1985

NASA

NASA Contractor Report 3924

A Theoretical Study of Non-Adiabatic Surface Effects for a Model in the NTF Cryogenic Wind Tunnel

J. M. Macha, L. A. Pare,
and D. B. Landrum
Texas A&M Research Foundation
College Station, Texas

Prepared for
Langley Research Center
under Grant NAG1-417

National Aeronautics
and Space Administration
Scientific and Technical Information Branch
1985

SUMMARY

A theoretical study has been made of the severity of non-adiabatic surface conditions arising from internal heat sources within a model in a cryogenic wind tunnel. Local surface heating is recognized as having an effect on the aerodynamic characteristics of the boundary layer. Variation of these characteristics can introduce changes in the flow about the model, and may affect the wind tunnel data. The purpose of the analysis is to compare the actual surface temperatures of the model with the temperatures that would exist on a perfectly insulated, adiabatic surface. The geometry was based on the NTF Pathfinder I wind tunnel model. A finite element heat transfer computer code was developed and used to compute the steady state temperature distribution within the body of the model, from which the surface temperature distribution was extracted. Particular three dimensional characteristics of the model were represented with various axi-symmetric approximations of the geometry. This analysis identified regions on the surface of the model susceptible to surface heating and the magnitude of the respective surface temperatures. The addition of insulation within the cavity to limit surface heating was also investigated. It was found that severe surface heating may occur in particular instances, but could be alleviated with additional insulating material. The heat flux through the surface of the model was integrated to determine the net heat required to maintain the instrumentation cavity at the prescribed temperature. The influence of the non-adiabatic condition on the boundary layer properties was shown to be marginally significant.

INTRODUCTION

The National Transonic Facility (NTF) at the NASA Langley Research Center is a technologically advanced wind tunnel which uses cryogenic nitrogen gas as the working medium. [1] The high Reynolds number capability of the NTF is achieved by operating at high total pressure and by injecting liquid nitrogen into the circuit to lower the gas temperature. Over the operating envelope of the wind tunnel, the minimum total temperature varies from 96K at one atmosphere to 122K at 8.8 atmospheres. Therefore, the NTF models and their instrumentation must be designed to tolerate cryogenic temperatures.

In the area of instrumentation, it has been determined that the Electronically Scanned Pressure (ESP) measuring system, which is mounted internally in the model, must be contained in a temperature controlled enclosure to maintain calibration. The recommended temperature range for the ESP system is 273K-350K. Likewise, the accelerometers that measure model pitch and roll must also be heated. [2]

An electrically-heated, thermally insulated instrumentation package has been designed for the Pathfinder I model, which is a generic, high aspect ratio transport configuration. The instrumentation unit is located in the forward portion of the fuselage. The heat conduction that occurs from the instrumentation package to the exterior of the model has the undesirable effect of creating a non-adiabatic surface which is unrepresentative of the atmospheric flight condition. It is well known that heat transfer at a fluid-solid boundary affects the development of the boundary layer and the magnitude of the surface shear stress. Therefore, there is a possibility that the aerodynamic characteristics of the model will not accurately simulate those of the full-scale aircraft. The severity of these effects depends on the ratio of model surface temperature to the freestream total temperature. Numerical calculations reported in Reference 3 show that turbulent friction drag on a flat plate is reduced by approximately 10% for a surface-to-total temperature ratio of 1.25. The quantitative effect of a heated wall on boundary layer stability is not precisely known, but a change in the location of transition of a few percent of the fuselage length could measurably alter the overall drag. The effect on boundary layer separation is not of consequence for the Pathfinder I model since the heating is confined to regions of favorable or mildly-adverse pressure gradient on the forward fuselage.

The actual variance of the surface temperature from the adiabatic value is determined by the following factors: the magnitude of the convective heat transfer coefficient; the heat conduction characteristics of the model structure; the thermal conductivity and thickness of the insulation material; and the heating requirements of the instrumentation package. A theoretical analysis has been made to determine the steady-state surface temperatures for simplified instrumentation cavity configurations, and for typical NTF operating conditions. The resulting deviations in friction drag and boundary layer thickness, as well as the total heat loss rates, have been calculated. The various axi-symmetric analytical models considered provide a conservative estimate of the non-adiabatic effects and heating requirements for the Pathfinder I wind tunnel model.

SYMBOLS

$[B]$	=	Spatial derivatives of shape function.
C_p	=	Pressure Coefficient.
H	=	Stagnation enthalpy.
h	=	Convective heat transfer film coefficient.
$[h_T]$	=	Element "stiffness" - convection.

$[H_T]$ = Global "stiffness" - convection.

$[k]$ = Thermal conductivity matrix.

$[k_T]$ = Element "stiffness" - conduction.

$[K_T]$ = Global "stiffness" - conduction.

L = Body length, 1.27 m

M = Mach number.

$[N]$ = Element shape functions.

P_o = Total, or stagnation, pressure.

q_w = Wall heat flux.

r = Element "force" matrix due to convection, or Adiabatic recovery factor.

R = Global "force" matrix due to convection.

Re_L = Reynolds Number based on body length.

r,z = Axi-symmetric coordinates.

s,n = Coordinates in element computational space.

S_c = Element edge with convection boundary.

T = Static temperature of fluid.

T_o = Total, or stagnation, temperature.

T_{aw} = Adiabatic surface temperature.

Te = Element nodal temperatures.

T_r = Convective fluid reference temperature.

T_w = Surface temperature.

x/L = Non-dimensional body length.

γ = Ratio of specific heats.

Note: The subscript "∞" implies free stream conditions for fluid flow parameters.

BACKGROUND ON NON-ADIABATIC SURFACE EFFECTS

The influence of heat transfer on the boundary layer at a fluid-solid interface depends on (1) the direction of heat flow; (2) the streamwise pressure gradient; and (3) the temperature-viscosity relationship for the particular fluid. The direction of heat flow is determined by the magnitude of the surface temperature T_w, relative to the adiabatic wall temperature

$$T_{aw} = T_o\left[1 + .5\, r(\gamma-1)M^2\right]\left[1 + .5(\gamma-1)M^2\right]^{-1} \qquad (1)$$

where M is the local Mach number outside the boundary layer and r is the recovery factor. For air or gaseous nitrogen, $r \simeq .85$ for laminar flow and $r \simeq 0.88$ for turbulent flow. The local heat flux can be expressed in terms of the convective film coefficient, h, and the temperature difference as

$$q_w = h\left[T_w - T_{aw}\right] \qquad (2)$$

The film coefficient can be determined from boundary layer calculations for specified flow and temperature conditions, and is only slightly dependent on the magnitude or sense of the temperature difference.

For flows of air or nitrogen, viscosity increases with temperature. In this case, the early theoretical work of Lees and Lin [4] demonstrated that a hot surface has a generally destabilizing effect on the boundary layer, in the absence of a streamwise pressure gradient. Conversely, a cold wall stabilizes the flat plate boundary layer.

The influence of heat transfer on flows with pressure gradient is elucidated by performing the Illingworth-Stewartson transformation on the boundary layer momentum equation (e.g., see Schlichting [5], Chapter XIII). The transformed differential equation differs from the corresponding adiabatic, incompressible equation merely by the ratio of local to freestream stagnation enthalpy, H/H_∞, which multiplies the pressure gradient term. In the vicinity of the wall, $H/H_\infty \gtrless 1$ for $T_w/T_{aw} \gtrless 1$. In effect, the non-adiabatic condition either enhances or degrades the significance of the pressure gradient, relative to the viscous and inertial terms, depending on the direction of heat flow. A hot surface accentuates the pressure gradient term, which increases laminar skin friction and the heat transfer film coefficient in regions of strongly accelerating flow, but decreases these parameters and promotes instability in mildly accelerating, neutral and decelerating regions. For turbulent flows, numerical solutions (e.g., References [3], [10]) show that a hot surface decreases skin friction in neutral and decelerating regions.

Reference [6] is a collection of articles which demonstrate the effects of a hot wall on boundary layer stability and transition Reynolds number. Reference [7] considers the maintenance of laminar flow along a wing by cooling the surface. Cohen and Reshotko [8] and Morduchow and Grape [9] relate the laminar separation point to wall heating or cooling. A combined numerical and experimental study by Norton, et al [10], demonstrated that a hot wall promotes turbulent separation and stall of an airfoil at low subsonic Mach number.

Potential non-adiabatic effects for the Pathfinder I fuselage were expected to be confined to (1) a reduction of skin friction in local regions of high temperature ($T_w > T_{aw}$) aft of the minimum pressure point; (2) an increase in the boundary layer displacement thickness; and (3) a movement of the laminar-to-turbulent transition location.

METHOD OF ANALYSIS

This analysis of the Pathfinder I wind tunnel model emphasizes the conditions within the operating envelope that result in the largest discrepancies from the adiabatic surface temperature, or the greatest internal heating requirements. By Reynolds Analogy, the film coefficient, h, for a turbulent boundary layer is proportional to Reynolds number raised to a power near unity. For fixed Mach number and total temperature, Reynolds number is directly proportional to the tunnel total pressure. Thus, the maximum values of h and the most severe power requirements to maintain specified internal cavity temperature occur at the highest tunnel stagnation pressure of approximately 9 atmospheres. On the other hand, the highest exterior surface temperatures occur for the lowest tunnel pressure.

Formulation of the analytic model is straight forward, except for the specification of the thermal environment of the instrumentation cavity within the fuselage. Here, two alternate approaches are plausible. In the first, a constant temperature within the tolerable range of the ESP system (300K, for example) is specified for the internal cavity that surrounds the instrumentation. This is a realistic simulation in the sense that the power to the heating elements in the actual model will be modulated to maintain a nearly constant temperature, as monitored by thermocouples attached to the package. The total power required to maintain the specified cavity temperature is found by integrating the heat fluxes around the cavity. This approach does not model the mild temperature gradients which will exist through the package, particularly for non-zero angles of attack where there is differential convection on the windward and leeward sides of the model. However, this effect should be negligible for the small angles of attack of interest.

The alternate approach is to specify discrete heat sources in the numerical model at locations that are representative of the heating elements in the actual model. This situation permits the thermal gradients through the package to exist, at the added computational expense of simulating the complicated heat conduction paths through the instrumentation unit. A further disadvantage of this approach is that the strength of the heat sources that will produce a tolerable cavity temperature must be found by an iterative procedure. Based on these considerations, the first condition described (that is, specified cavity temperature) was used in the analysis.

Several axi-symmetric configurations were used to model the more-complicated, three-dimensional geometry of the cavity. The approximate configurations lead to results that bound the thermal characteristics of the actual geometry. The analyses were performed for a freestream Mach number of 0.6, stagnation temperature of 100^{o}K, and stagnation pressures of two and nine atmospheres.

The five steps used in the analysis are:

1. Determine the inviscid pressure distribution over the forward fuselage for zero angle of attack using available potential flow computer codes.

2. Calculate the streamwise distribution of the convective heat transfer coefficient assuming an isothermal, slightly non-adiabatic surface condition, using available boundary layer codes.

3. Input the heat transfer coefficients and the specified cavity temperature into a finite element thermal analysis code that has been tailored to the model geometry, and calculate the steady state surface temperature distribution.

4. If necessary, repeat steps 2 and 3 using the new, non-isothermal surface temperatures. One iteration should be sufficient.

5. Evaluate the deviation of the boundary layer properties relative to the adiabatic condition, and the total heat loss rate.

ANALYTIC MODEL OF THE PATHFINDER I

Physical Description

The Pathfinder I, shown in Figure 1, is a generic model intended to represent a typical high aspect ratio air transport. The model has modular construction to permit variations about a basic configuration. The components and dimensions of the model are shown in Figure 2. The forward fuselage section houses the

instrumentation package, which includes accelerometers and pressure sensing devices, along with their respective heating elements as shown in Figure 3. The accelerometer package contains internal heater elements which maintain the sensors at 160°F. The pressure sensing device is surrounded by a cylinder with electrical resistance heating strips mounted on the inner surface. Additional heating elements are located on a cap which closes the forward end of the cylinder assembly. The instrumentation package is surrounded by an insulating liner which fits inside the forward fuselage shell, as shown in Figure 4. The body of the Pathfinder I is stainless steel, and the liner is composed of a closed-cell foam cryogenic insulator.

The fuselage geometry and the arrangement of heat sources in the cavity are such that an axi-symmetric model is sufficiently representative of the actual Pathfinder I, except for the metal structure that supports the instrumentation package. This support, which can be seen in Figure 3, provides a thermal path from the base of the accelerometer package to the bulkhead at the back of the cavity.

The analytic model, which is shown in Figure 5, consists of a stainless steel outer shell in the forward section, and a solid steel aft body. Contained within the forward shell is the insulation liner which surrounds the cavity. A region which represents the air space between the accelerometer package and the interior surface of the insulation liner has been incorporated into the model. Alternately, assigning this region the thermal properties of steel provides a conservative estimate of the effect of the support structure. Along the exposed steel surfaces at the aft end of the cavity, a thin layer for which arbitrary material properties may be specified has been defined. This layer permits investigation of the effect of additional insulation to inhibit heat conduction to the surface. Perfect thermal contact is assumed to exist at all material interfaces.

Conservative values for the thermal properties of the materials which comprise the wind tunnel model are given in Table 1. They are assumed to be constant with respect to temperature. The rational of this assumption is discussed in a later section.

Table 1

Material Properties

Material	Thermal Conductivity (W/m-K)
Stainless steel	14.0
Insulation	0.006
Air space (natural convection)	0.130

Finite Element Model

Although the finite element method is most often used for structural analysis and solid mechanics applications, it is well suited to many other classes of problems. Among these are the potential field problems which include heat transfer, diffusion in porous media, and electrical and magnetic potential fields [11].

Finite element analysis has several advantages over most finite difference schemes. These include the simple application of non-homogeneous and/or anisotropic material properties, natural introduction of specified gradient and prescribed value boundary conditions, element size grading to provide high accuracy in critical regions, and the availability of higher order elements. Furthermore, the computational techniques and solution schemes are similar for most types of finite element applications. For these reasons, a finite element approach to the thermal analysis was selected.

A 2-D or axi-symmetric heat transfer code using the finite element method was developed by the second author. The eight-node isoparametric quadrilateral element was selected for use in the code [11, 12]. This element, illustrated in Figure 6, has several benefits, including easy modifications into axi-symmetric form and curvilinear shape allowing greater flexibility in grid development. Isoparametric elements permit variation of boundary conditions along element edges, yielding a more accurate modeling of the problem. The finite element code was developed to analyze linear, steady-state problems with material properties that do not vary with respect to temperature.

The intermediate steps from the differential heat conduction equation to the finite element formulation are provided in References [11, 12] and are not repeated here. The global system of equations for the finite element analysis is:

$$\left(\left[K_T\right] + \left[H_T\right]\right)\left\{T\right\} = \left\{R_\infty\right\}. \tag{3}$$

For a single element the temperature field is described by

$$T = \left[N_T\right]\left\{T_e\right\}, \tag{4}$$

where $[N_T]$ is the vector of element shape functions, and $\{T_e\}$ are the nodal temperatures. The derivatives of the shape functions are expressed as

$$[B_T] = \left\{ \partial/\partial r \quad \partial/\partial z \right\} [N_T] \ . \tag{5}$$

The element conductive stiffness is defined by

$$[k_T] = \int [B_T]^T [k] [B_T] \, r \, ds \, dn \tag{6}$$

where [k] is the conductivity matrix. The contribution to the element stiffness due to convection is given by

$$[h_T] = \int [N_T]^T [N_T] \, h \, r \, dS_c \tag{7}$$

and the element force due to convection is

$$\{r_\infty\} = \int [N_T]^T \, h \, T_r \, r \, dS_c \ . \tag{8}$$

Here, S_c is the element edge with the convective boundary, h is the convective heat transfer film coefficient and T_r is the fluid reference temperature. T_r is taken to be the adiabatic wall temperature. Numerical integrations were carried out using a three-point Gauss quadrature scheme.

The thermal analysis code was verified by the evaluation of several check cases. These cases were "textbook" type heat transfer problems with known exact solutions, and are described in the Appendix. They included plane walls, thin walled cylinders, and spherical shells with prescribed temperatures, perfect insulation and/or convection boundary conditions. Each problem was evaluated by an appropriate finite element model of the geometry and boundary conditions. As a result of these check cases confidence was established in the ability of the code to provide accurate solutions to two-dimensional and axi-symmetric heat transfer problems. On this basis, the thermal analysis code is expected to yield realistic solutions for the substantially more complex geometry and boundary condition combinations presented by the Pathfinder I.

The grid shown in Figure 7 was developed to represent the NTF Pathfinder I. This grid has groups of elements which represent the various materials and their respective geometries as defined in the analytic model. Where possible, the grid pattern was designed to approximate the pattern of isotherms and adiabats that might be expected to exist in the body, so that the accuracy of the results might be enhanced [12]. Additionally, the size and number of elements was adjusted to increase the resolution of the solution in potentially critical regions (i.e., areas of thin insulation and the aft end of the cavity).

The accuracy of a finite element analysis depends in part, upon the number of elements used and the degree to which the finite element model represents the actual article. The number of elements is restricted by the memory and computational limits of the available computer. Also, simplified geometries were used to reduce the magnitude of computation(i.e., axi-symmetric vs. fully 3-D).

RESULTS AND DISCUSSION

Pressure Distribution

Surface pressure distributions for the Pathfinder I fuselage were calculated with two different potential flow methods. The Hess panel code [13, 14] was used for initial computations for both zero and small angles of attack. The zero angle of attack pressure distributions were also calculated with the full potential transonic code "WEDAN", by Langley Research Center personnel.

The Hess code is an inviscid, potential flow panel method which represents lifting surfaces by horseshoe vortices and nonlifting volumes by doublets. The method uses the standard Prandtl-Glauret correction for compressible subsonic flow conditions. Figure 8 illustrates the fuselage geometry modeled, and the streamwise location of control points in the nose region. Based on several trial computations, it was decided that sufficient accuracy was obtained by using fourteen panels around the semi-circumference of the fuselage.

Figure 9 shows the resulting axial pressure distributions for incompressible flow ($M_\infty = 0$), for angles of attack of 0° and 10°. For the 10° case, the pressures shown are those along the uppermost row of panels (approximately six degrees away from the vertical plane of symmetry). The notable feature of the curves is the local, abrupt region of recompression very near the nose. This phenomenon is apparently caused by the bluntness of the spherical nose, followed by the basically ogive shape. The local region of decelerating flow can be expected to influence the location of laminar-to-turbulent transition.

Pressure distributions have also been calculated with a full-potential transonic code called "WEDAN", for zero angle of attack, and Mach numbers of 0.6 and 0.84. The computations were performed by Langley Research Center (LaRC) personnel and forwarded to Texas A&M for use in this research. The results of the "WEDAN" calculations are shown in Figures 10 and 11. Like the Hess code solutions, these data also predict a local region of deceleration at the spherical-nose-ogive junction. For $M_\infty = 0.84$, the sonic point is reached at $x/L \simeq 0.09$. A comparison of the "WEDAN" and Hess code results for $M_\infty = 0.6$ shows that the Prandtl-Glauert correction underestimates the increase in the magnitude of C_p due to compressibility.

Boundary layer calculations based on the integral method of Walz [15] were carried out to investigate the effect of the recompression region near the nose on the transition process. The location of the neutral stability point is determined by comparing the local Reynolds number based on boundary layer thickness to a critical value calculated from linear stability theory for a one-parameter family of velocity profiles. The neutral stability point is the upstream bound for the actual transition point. Calculations were made for the Mach 0.6 pressure distribution and an adiabatic wall condition, over a Reynolds number range of $10^6 - 10^9$. The results, which are presented in the second column of Table 2 and in Figure 12, show that for $Re_L \geq 10^7$ the point of neutral stability occurs in the recompression region. For comparision, a smoothed C_p distribution with the recompression eliminated was also investigated. These results are presented in Table 2 and in Figure 13, and show an orderly forward migration of the instability point with increasing Reynolds number. For the Pathfinder I pressure distribution, there is no way to accurately calculate the actual transition point. However, there is a strong possibility that the recompression will effectively "trip" the boundary layer at the higher Reynolds numbers of interest. On this basis, the transition point for all subsequent boundary layer calculations was fixed at $x/L = .007$, coinciding with the recompression region.

Table 2

Neutral Stability Location for Pathfinder I Fuselage
at Various Reynolds Numbers

Re_L	x/L Neutral Stability (Actual Cp)	x/L Neutral Stability (Smoothed Cp)
$1x10^6$	0.14095	0.14095
$1x10^7$	0.0061	0.12209
$1x10^8$	0.00547	0.04210
$5x10^8$	0.00525	0.00716
$1x10^9$	0.00413	0.00572

Convective Heat Transfer

Surface distributions of the convective heat transfer film coefficient, h, were calculated for a range of specified wall temperatures and freestream conditions, using the boundary layer code by Anderson and Lewis [16]. This code uses an implicit finite-difference scheme to solve the laminar, transitional, and/or turbulent boundary layer equations. The accuracy of the code for cryogenic nitrogen and adiabatic conditions has been verified by comparison with experiment [17]. The code has also been used to predict the thermal stabilization time for models in the NTF, following a change in the tunnel total temperature [18].

The results for the film coefficient for the Pathfinder I fuselage are shown in Figure 14. The data presented are for freestream conditions of $M_\infty = 0.6$, $T_O = 100K$, and $P_O = 2$ and 9 atmospheres. The several curves for the 9-atmosphere condition show that the value of h is sensibly constant over a range of wall temperatures of $1.0 \leq T_W/T_O \leq 1.5$. Based on these results, the film coefficient distributions corresponding to $T_W/T_O = 1.2$ were used subsequently in the finite-element heat conduction analysis, irrespective of the actual surface temperature values.

Thermal Analysis

The finite-element thermal analysis of the Pathfinder I wind tunnel model and the resulting surface temperature distributions are discussed in this section. Five axi-symmetric internal geometries were modeled by altering the material thermal property designations of the basic element grid shown in Figure 7. The geometries investigated were designed to bound the influence of the three-dimensional aspects of the accelerometer heat source, and to evaluate the effects of additional insulation. The configurations analyzed, labeled I, II, III, IV and V, are illustrated in Figures 15, 16 and 17 and are discussed below.

Configurations I and II: These two configurations assume the entire cavity is at a constant 300K. Configuration I reflects the existing insulation in the Pathfinder I model. Configuration II is identical to I, except insulation has been added to the exposed steel walls in the aft portion of the cavity.

Configurations III and IV: Additional elements have been added to account for the air gap between the accelerometer package and the insulation. There are now two heat sources: the forward portion of the cavity, and the surface of the accelerometer package. Both are assumed to be at 300K. Configuration III reflects the existing insulation in the Pathfinder I model, but includes the air gap. Configuration IV is identical to III except that it adds insulation to the steel surfaces at the aft end of the cavity.

Configuration V: This configuration, based on the element grids of III and IV, was developed to study the effects of the steel bracket that supports the accelerometer package in the Pathfinder I. The bracket can be seen in Figure 3 and is located beneath the accelerometer package and extends downward to conform with the interior shape of the insulation liner. Using the radial dimensions of the bracket within the cavity, an axi-symmetric approximation was created. Insight on the heat conduction through the bracket, into the body, and to the outer surface of the model is gained through analyzing this configuration.

Temperature Distribution

The fuselage temperature distributions for the five cavity configurations were evaluated using the finite-element thermal analysis code. Figures 18-22 show the distribution of temperature throughout the model for freestream conditions of Mach 0.6 and two-atmospheres total pressure. The illustrations were created by displacing each node point vertically by an amount corresponding to its temperature. The base plane in each figure shows the finite-element grid for reference.

For Configuration I (Figure 18), the steel surface at the aft end of the cavity is exposed directly to the 300K environment, and the heat is readily conducted to the outer surface of the model. The maximum surface temperature in this region exceeds the adiabatic surface temperature by over 100K. However, by adding a layer of insulation to the aft wall of the cavity (i.e., Configuration II in Figure 19), the heat conduction to the outer surface is drastically reduced.

With Configuration III, shown in Figure 20, the air gap that completely surrounds the heated accelerometer unit provides sufficient thermal resistance to keep the surface temperature very near the adiabatic value. The temperatures for Configuration IV (Figure 21) differ from those of Configuration III by only fractions of a degree.

The results for Configuration V are shown in Figure 22. The steel annulus, which is the axi-symmetric representation of the support bracket, provides a conduction path to the exterior surface of the model. The maximum surface temperature is approximately 40K above the adiabatic value. In the actual Pathfinder I, the support bracket is located only along the lower portion of the cavity, with air space on the top and sides. This geometry should direct the heat conduction downward, and result in even higher temperatures on the under-side of the fuselage. However, the nearby wing attachment may serve as a heat sink to limit the surface temperature.

The temperature distributions along the outer surface are presented in Figures 23-28, for Configurations I, III and V, and for stagnation pressures of two and nine atmospheres. The higher convective film coefficient associated with the nine-atmosphere condition substantially reduces the maximum surface temperatures for Configurations I and V.

The heat flux at the outer surface was integrated over the entire surface of the model, yielding the total power required to maintain the 300K cavity environment. These values are presented in Table 3, for Configurations I, III, and V. The total heat loss rates for Configurations I and V are significantly greater for the nine-atmosphere condition, while there is negligible effect of freestream stagnation pressure for Configuration III.

Based on these results, the value of 32 watts for Configuration III can be taken as a lower bound on the heating requirements for the Pathfinder I. It is also evident, from the results for Configuration V, that the heat conduction through the steel support bracket will cause the actual power requirement to be considerably greater. Furthermore, the most severe heating requirement is on the accelerometer unit, which is attached directly to the support bracket. This situation can be improved by placing a layer of insulating material between the accelerometer unit and the support.

Table 3

Total Heat Loss Rates

	Heat Loss Rate (watts)	
Configuration	2-atm.	9-atm.
I	2906.0	4064.0
III	32.1	32.0
V	822.0	906.0

Boundary Layer Calculations

The effects of the non-adiabatic wall temperature distributions on the boundary layer properties were calculated by the method of Anderson and Lewis [16]. Based on the results of the transition study discussed previously, the transition point for these calculations was fixed at the beginning of the recompression region near the fuselage nose.

The variations of the skin friction coefficient along the length of the body, for freestream conditions of Mach 0.6 and two-atmospheres stagnation pressure, are shown in Figure 29. The three curves correspond to the adiabatic temperature distribution, and to the two non-adiabatic distributions for Configurations I and V. The non-adiabatic temperatures produce a significant local reduction in C_F, relative to the adiabatic condition. However, the decrease in the total skin friction drag of the fuselage is less than two-percent for Configuration V, and less than one-half of one percent for Configuration I.

The variations of the boundary layer displacement thickness are shown in Figure 30. The relative increase in boundary layer thickness that occurs in the region of maximum surface temperature persists to the aft end of the fuselage.

CONCLUDING REMARKS

A theoretical analysis has been made of the severity and effect of non-adiabatic surface conditions for a model in the NTF cryogenic wind tunnel. The model geometry considered was the Pathfinder I, which is a generic transport design. The non-adiabatic surface condition arises from heat sources that are used to maintain a constant thermal environment for internal instrumentation. The analysis was made for several axi-symmetric representations of the instrumentation cavity, using a finite-element heat conduction code. Available potential flow and boundary layer codes were used to calculate the convective heat transfer boundary condition for the exterior surface of the model. The cavity region was assigned a constant temperature of 300K.

The results of the steady-state analysis for typical NTF freestream conditions showed that the surface temperature is significantly greater than the adiabatic value, in a region near the bottom, aft end of the cavity. It is likely that this undesirable situation can be eliminated by the addition of an insulating material between the heated accelerometer unit and its support structure. The thermal analysis also yielded a lower boundary of 32 watts on the power requirements to maintain the cavity at 300K.

The effects of the calculated surface temperature distributions on the skin friction drag and boundary layer displacement thickness were shown to be marginally significant. The maximum decrease in drag was less than two percent, compared to the adiabatic surface temperature condition.

REFERENCES

1. Howell, R. R.: The National Transonic Facility: Review and Status Report. High Reynolds Number Research - 1980, NASA CP-2183, December 1980, pp. 37-52.

2. Ladson, C. L.: Instrumentation for Calibration and Control of a Continuous Flow Cryogenic Wind Tunnel. High Reynolds Number Research - 1980, NASA CP-2183, December 1980, pp. 81-91.

3. Adcock, J. B. and Johnson, C. B.: A Theoretical Analysis of Simulated Transonic Boundary Layers in Cryogenic-Nitrogen Wind Tunnels. NASA TP-1631, March 1980.

4. Lees, L. and Lin, C. C.: Investigation of the Stability of the Laminar Boundary Layer in a Compressible Fluid. NACA-TN-1115, 1946.

5. Schlichting, H.: Boundary Layer Theory. 7th Edition, McGraw-Hill, New York, 1979, Chap. XIII.

6. Lin, C. C. (editor): Turbulent Flows and Heat Transfer. Vol. V. High Speed Aerodynamics and Jet Propulsion, Princeton University Press, Princeton, N. J., 1959, pp. 53-67, 102-110, 396-402.

7. Lekoudis, S. G.: Stability of the Boundary Layer on a Swept Wing with Wall Cooling. AIAA Journal, Vol. 18, September 1980, pp. 1029-1035.

8. Cohen, C. B. and Reshotko, E.: Similar Solutions for the Compressible Laminar Boundary Layer with Heat Transfer and Pressure Gradient. NACA-TN-3325, 1955.

9. Morduchow, M. and Grape R. G.: Separation, Stability and Other Properties of Compressible Boundary Layers with Pressure Gradient and Heat Transfer, NACA-TN-3296, May 1955.

10. Norton, D. J., Macha, J. M. and Young J. C.: Surface Temperature Effects on Subsonic Stall. Journal of Spacecraft and Rockets, Vol. 10, No. 9, 1973, pp. 581-7.

11. Zienkiewiez, O. C.: The Finite Element Method. McGraw-Hill Book Company UK Limited, London, 1972.

12. Cook, R. D.: Concepts and Applications of Finite Element Method Analysis. John Wiley & Sons, New York, N. Y., 1974.

13. Hess, J. L.: Calculation of Potential Flow about Arbitrary Three-Dimensional Lifting Bodies. Rep. No. MDC J5679/01, (Contract N00019-C-71-0524), Douglas Aircraft Co. Oct. 1972. (Available from DTIC as AD 755 480.)

14. Halsey, N. D.: A Three-Dimensional Potential Flow Program with a Geometry Package for Input Data Generation. NASA CR-145311 (Douglas Report MDC J7733), March 1978.

15. Walz, A.: Boundary Layer of Flow and Temperature. M.I.T. Press, Cambridge, Mass., 1969.

16. Anderson, E. C. and Lewis, C. A.: Laminar or Turbulent Boundary Layer Flows of Perfect Gases or Reacting Gas Mixtures in Chemical Equilibrium. NASA CR-1893, October 1971.

17. Johnson, C. B. and Adcock, J. B.: Measurement of Recovery Temperature on an Airfoil in the Langley 0.3-m Transonic Cryogenic Tunnel. Presented at the AIAA 16th - Thermophysics Conference, Palo Alto, CA, June 1981.

18. Johnson, C. B.: Theoretical Study of Nonadiabatic Boundary-Layer Stabilization Times in a Cryogenic Wind Tunnel for Typical Stainless-Steel Wing and Fuselage Models. NASA TM-80212, July 1980.

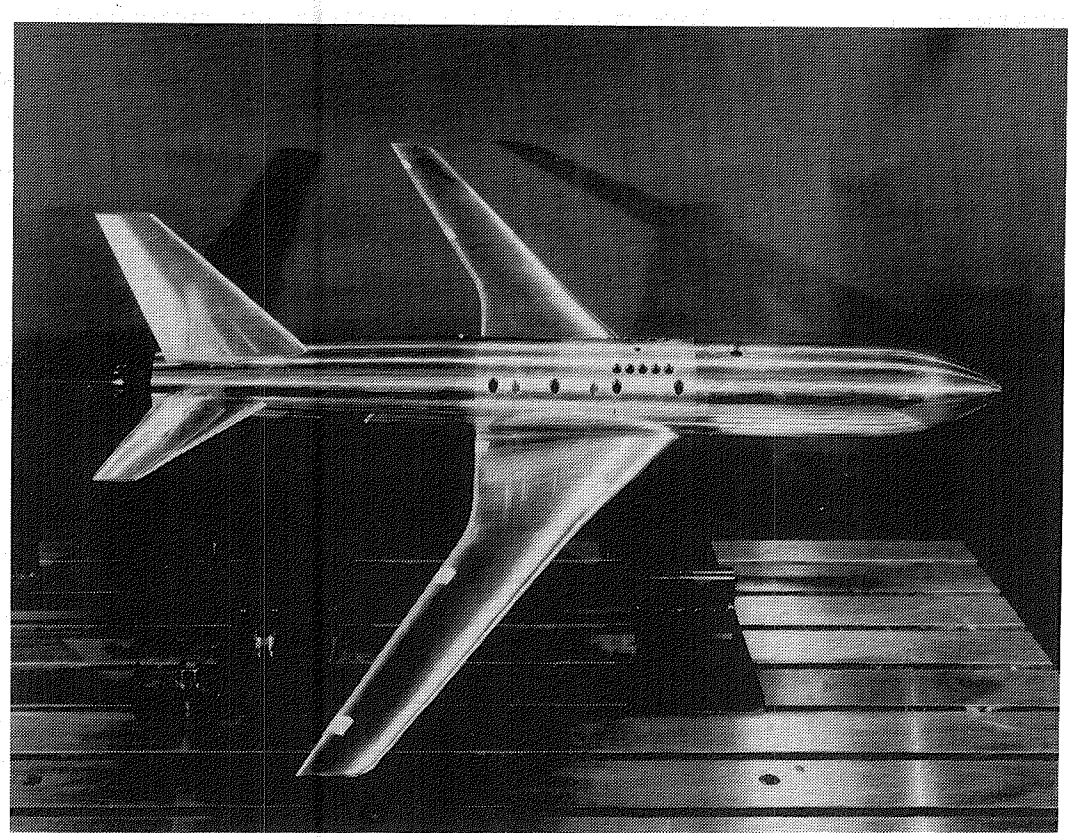

Figure 1. NTF Pathfinder I Wind Tunnel Model.

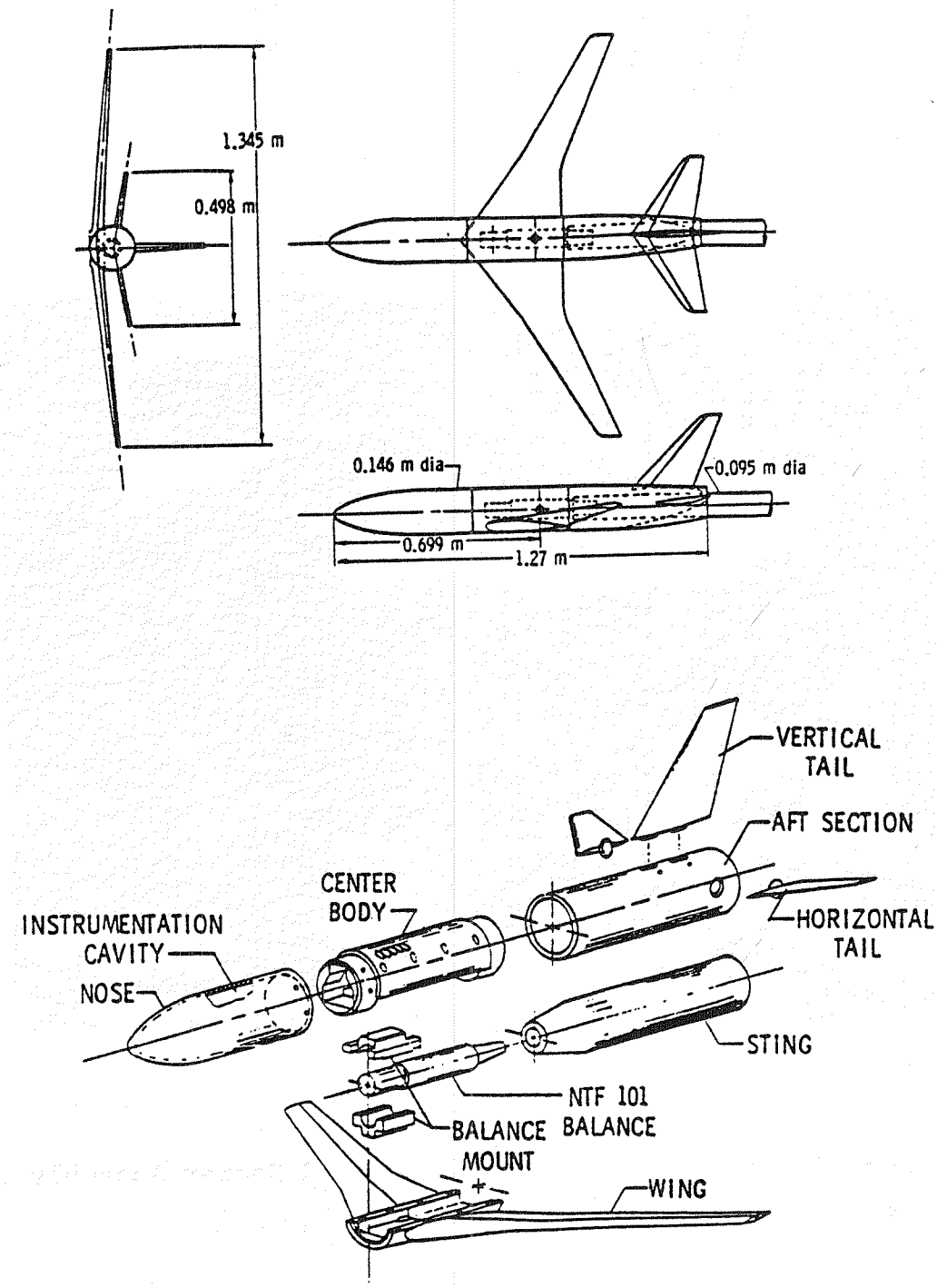

Figure 2. Pathfinder I Model Components and Dimensions.

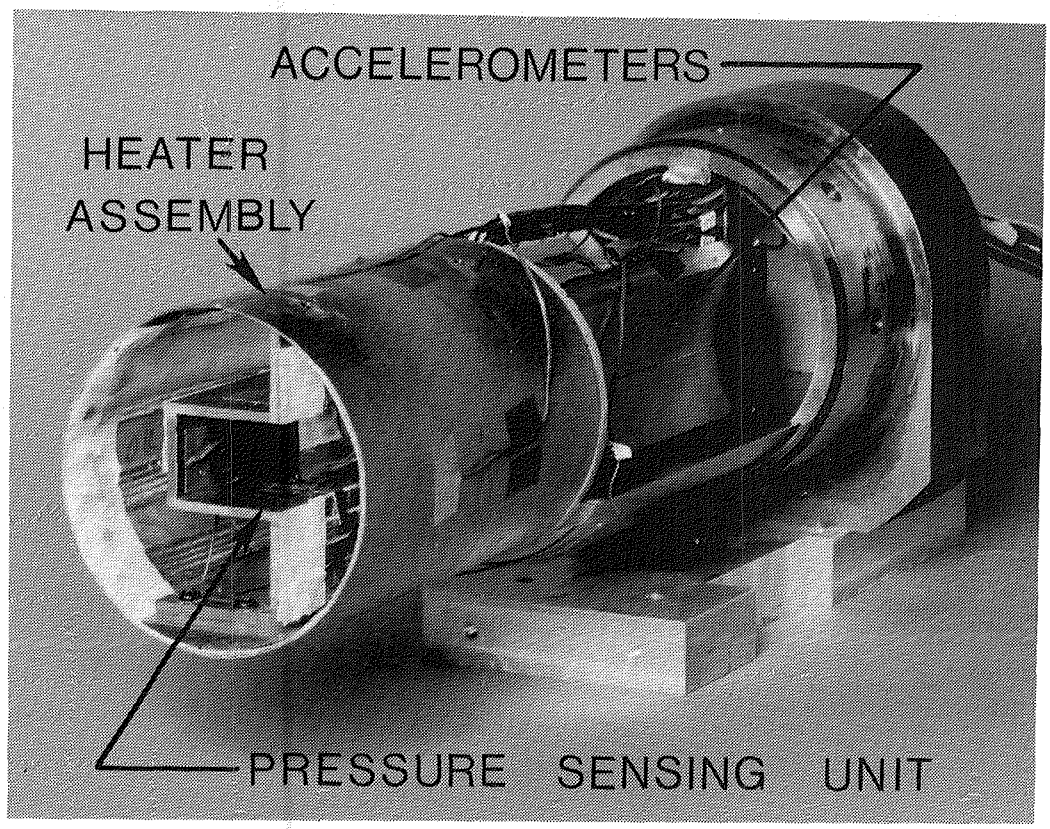

Figure 3. Instrumentation Package and Heater Assembly for Pathfinder I Model.

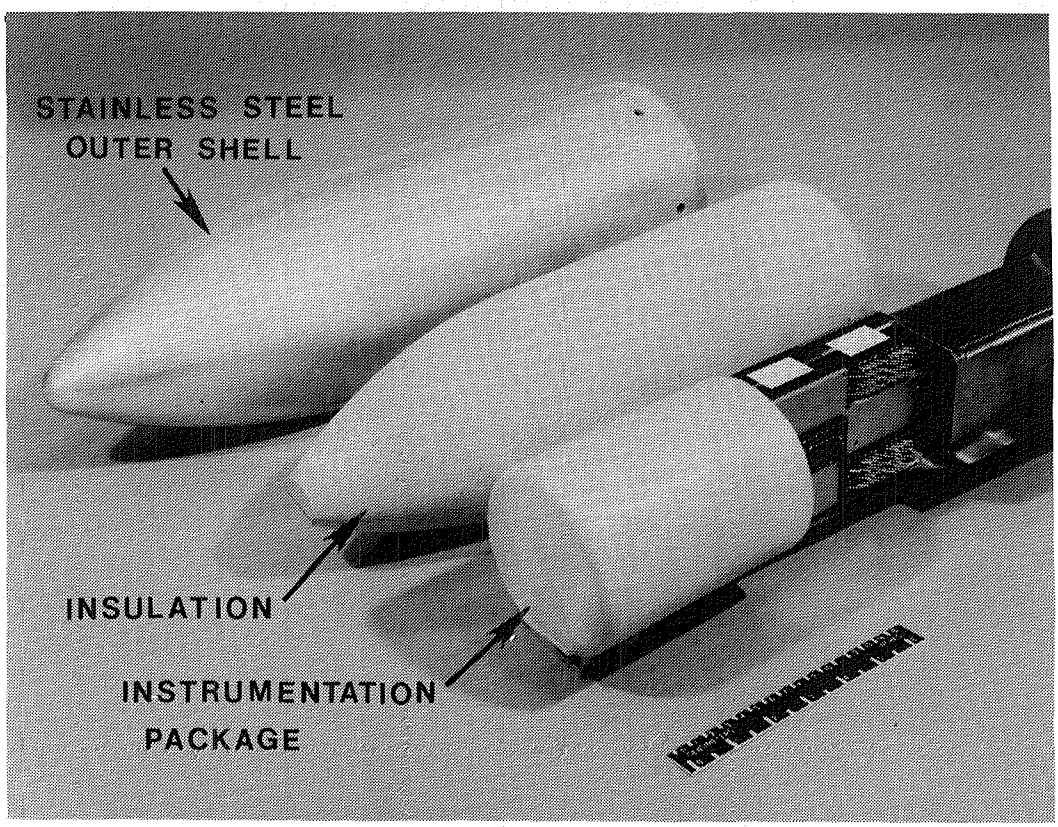

Figure 4. Forward Fuselage Shell (Stainless-Steel), Insulated Liner, and Instrumentation Package.

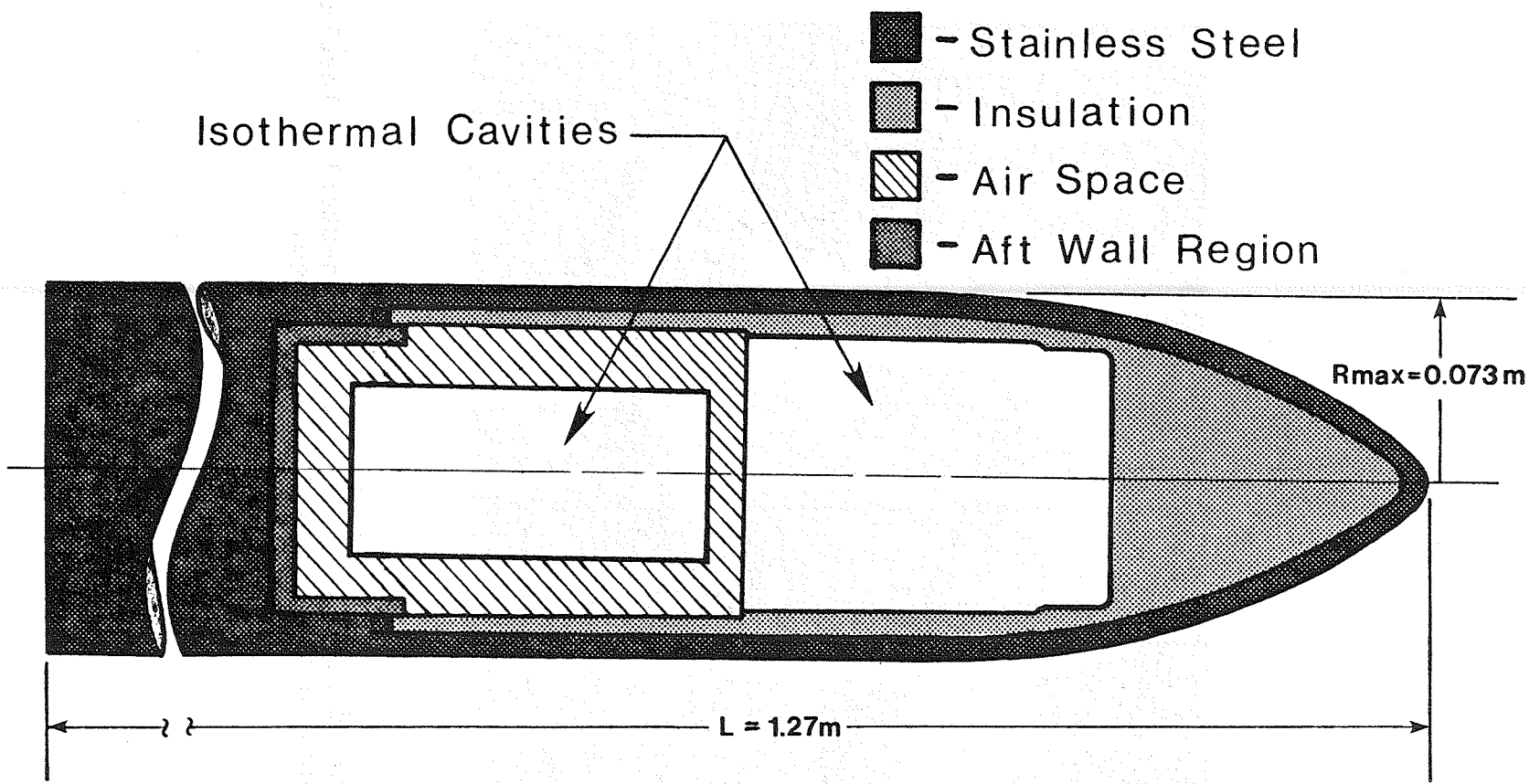

Figure 5. Analytic Model used to represent the Pathfinder I Wind Tunnel Model.

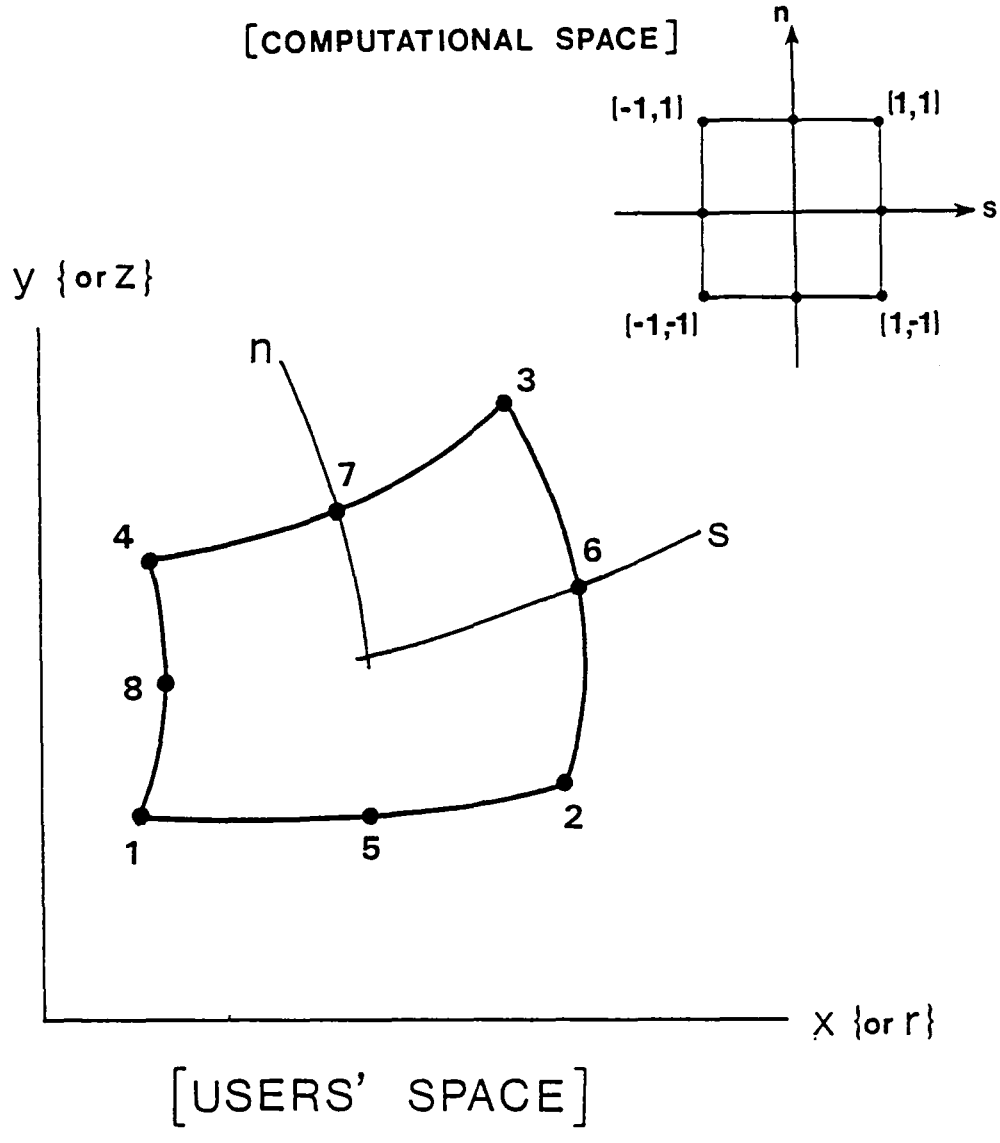

Figure 6. Eight Node Isoparametric Quad Element, as seen by the User, and Transformed Element for Computational Operations.

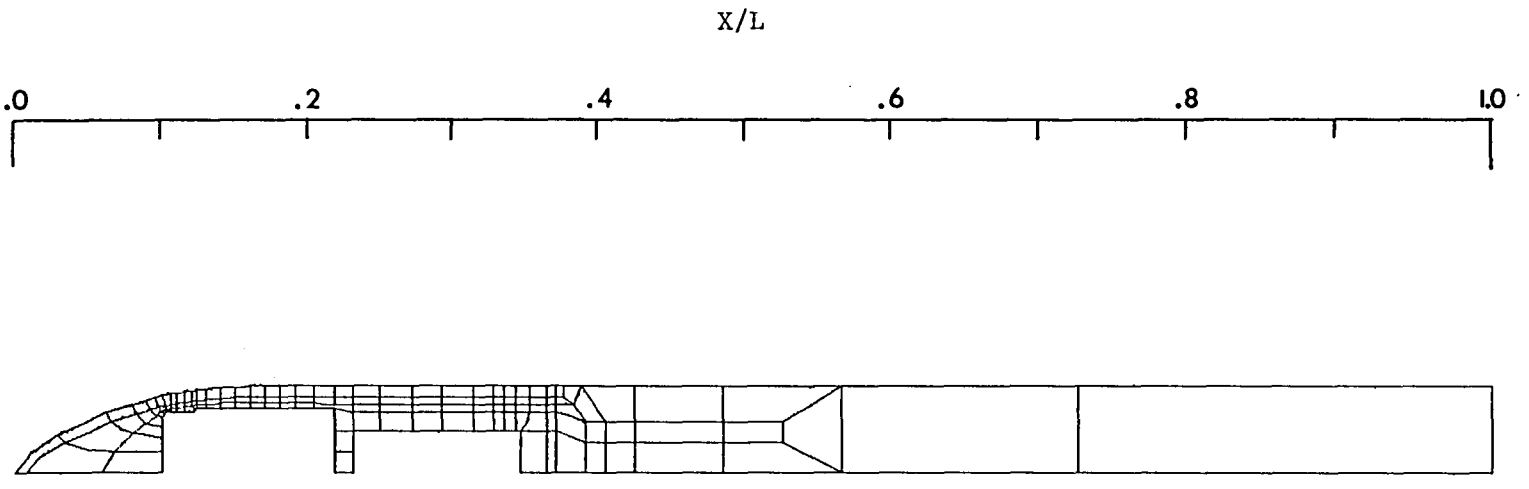

(a)

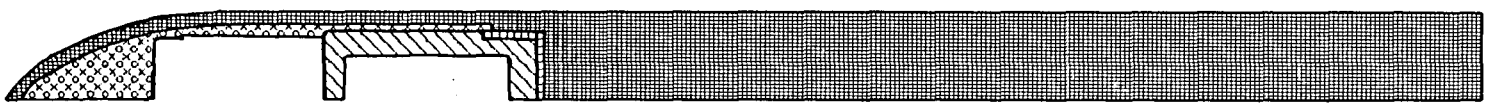

(b)

Figure 7. (a) Basic Finite Element Grid.
(b) Typical Thermal Analysis Configuration.

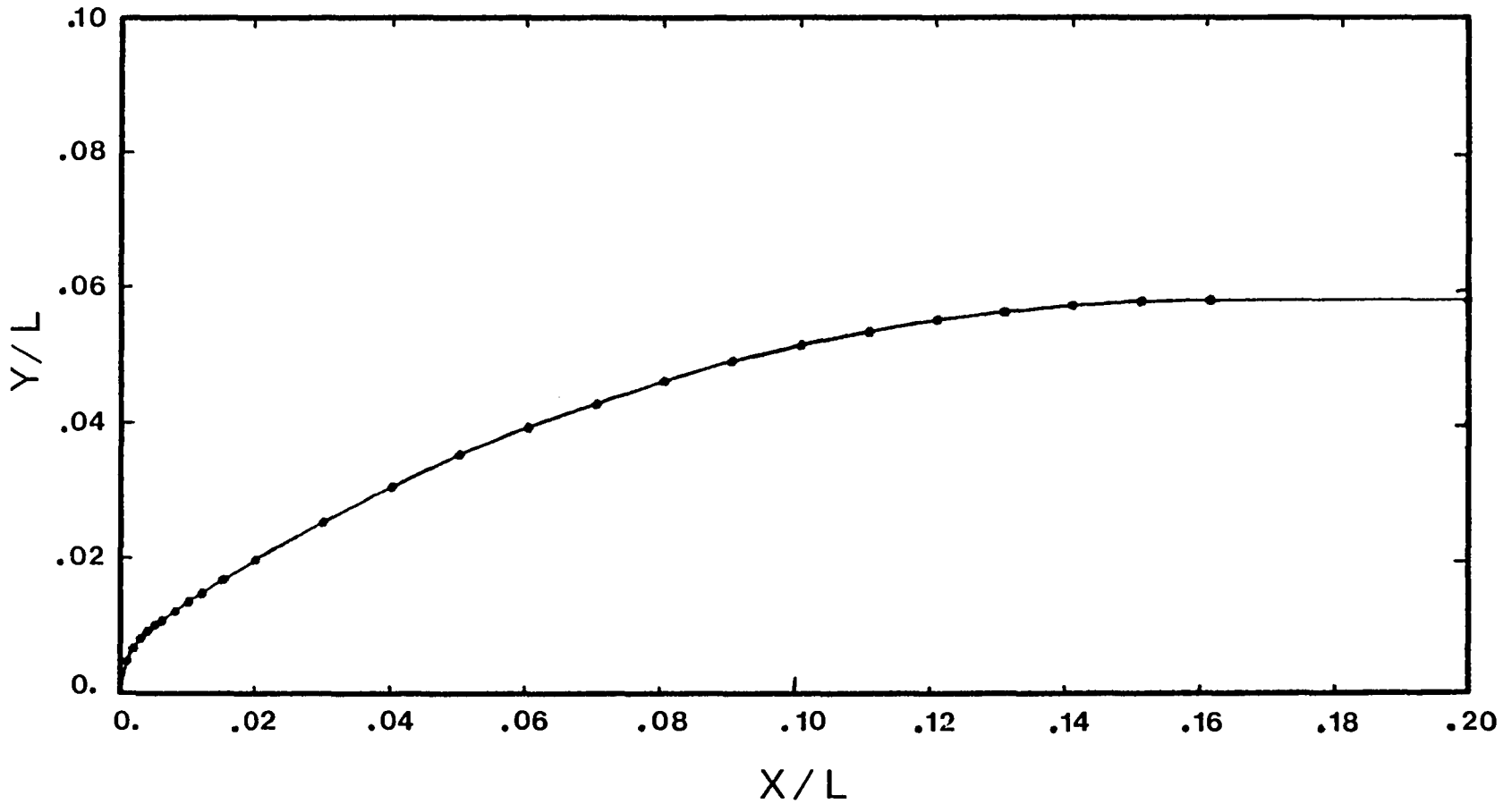

Figure 8. Fuselage Geometry and Panel Distribution used in the Nose Region for the Subsonic Potential Flow Code of Reference 13.

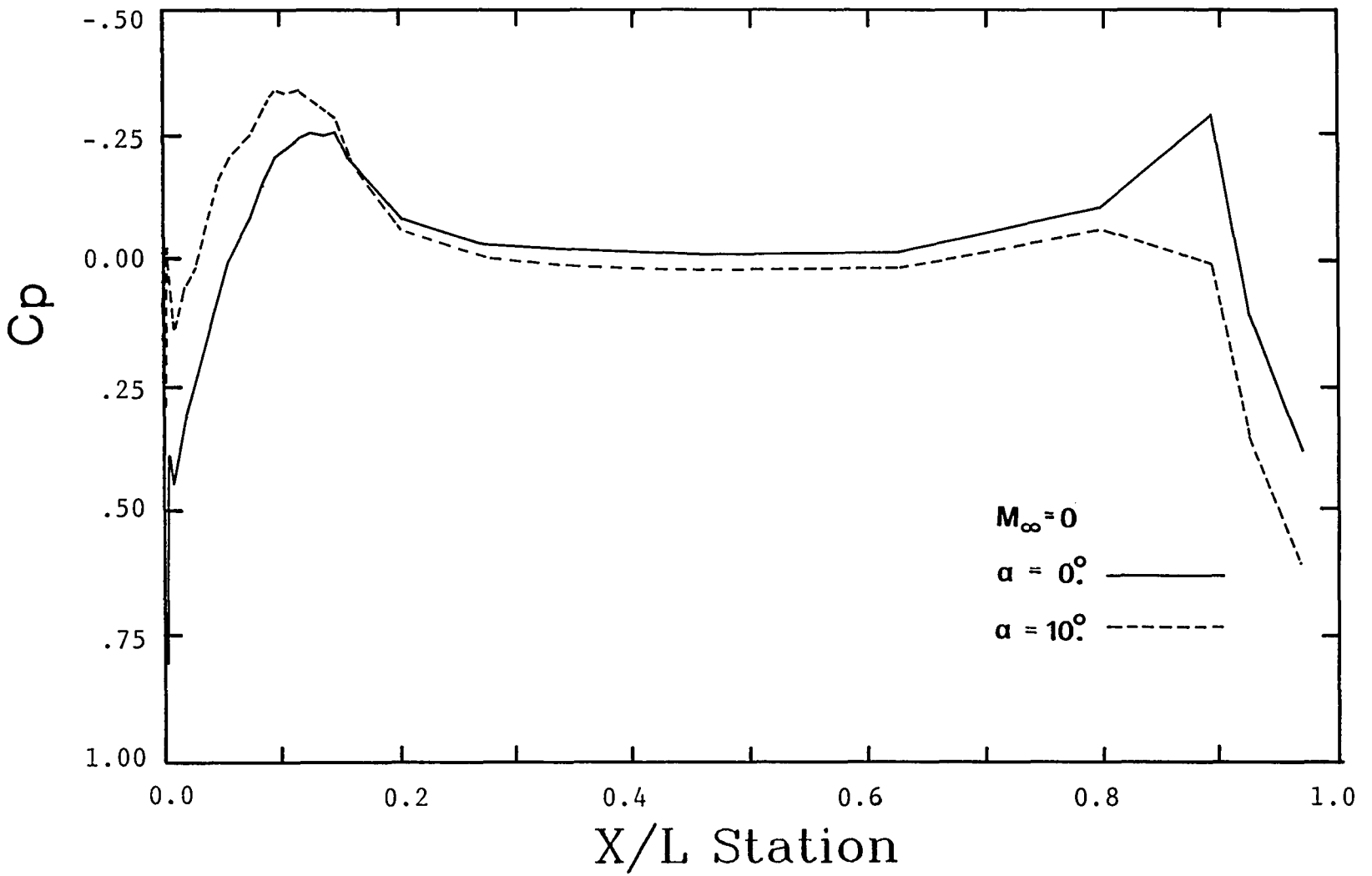

Figure 9. Calculated Pressure Distributions for the Pathfinder I Fuselage Based on the Subsonic Potential Flow Code of Reference 13.

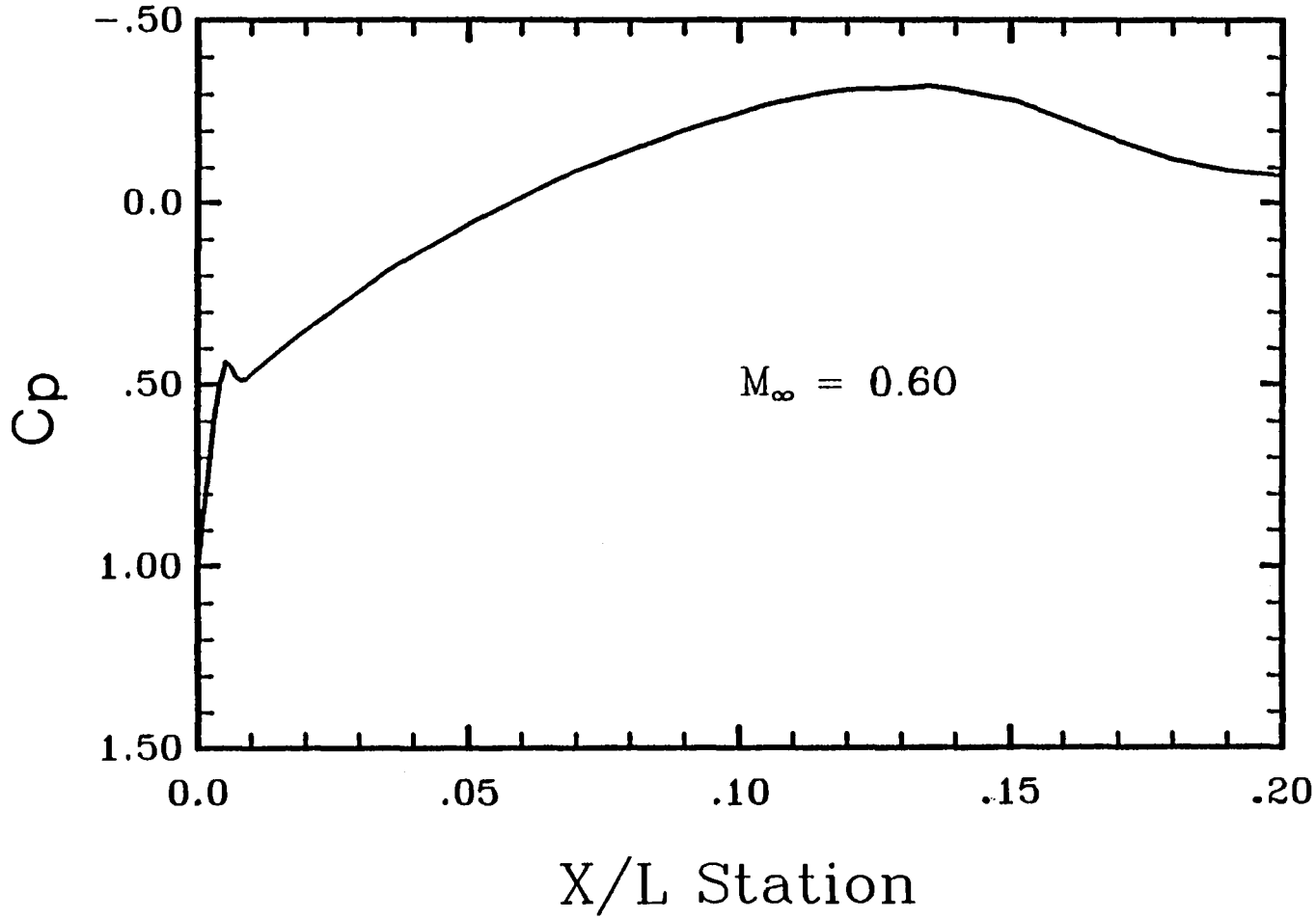

Figure 10. Pressure Distribution from "WEDAN" Code for the Pathfinder I for Mach Number of 0.60.

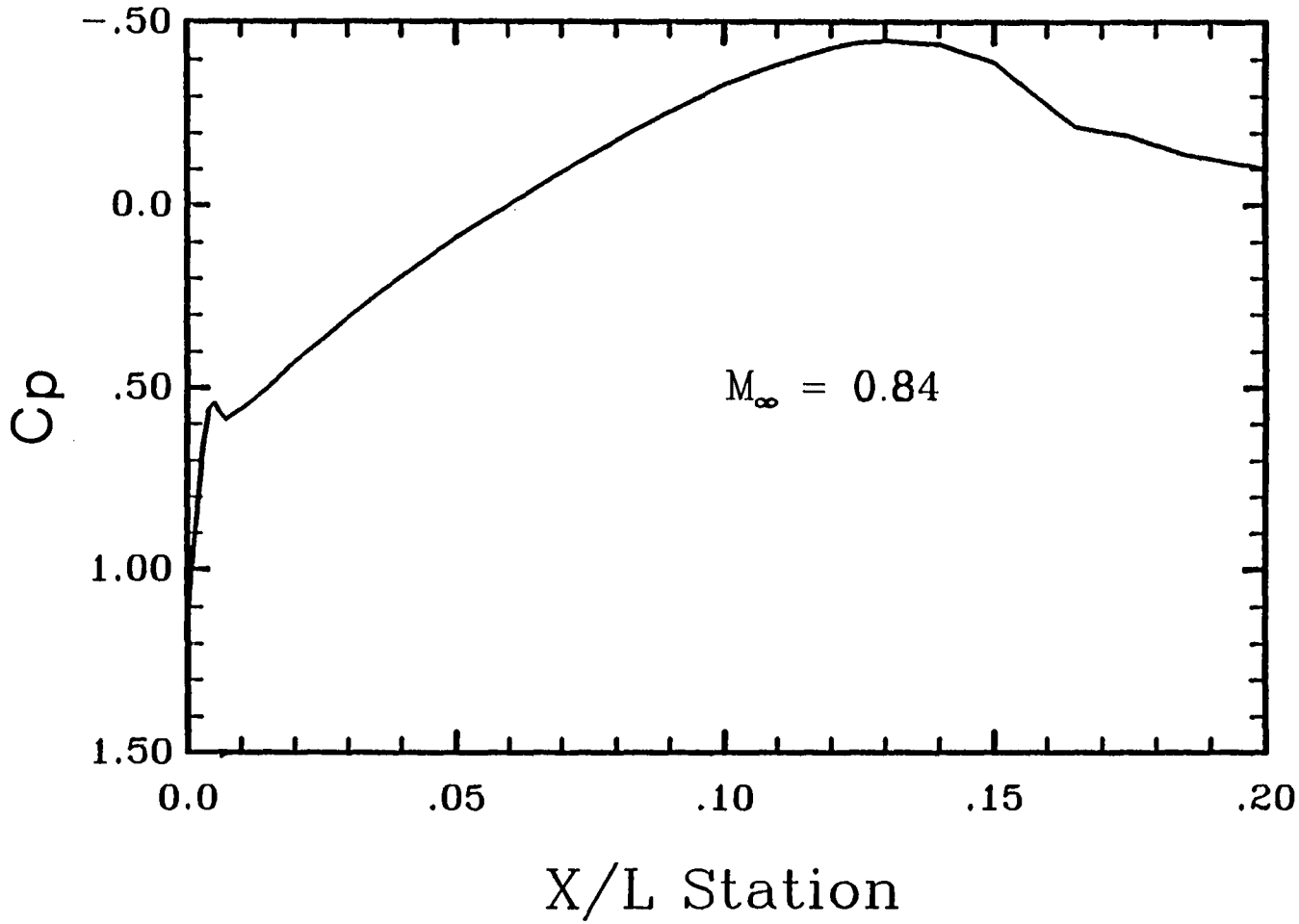

Figure 11. Pressure Distribution from "WEDAN" Code for the Pathfinder I for Mach Number of 0.84.

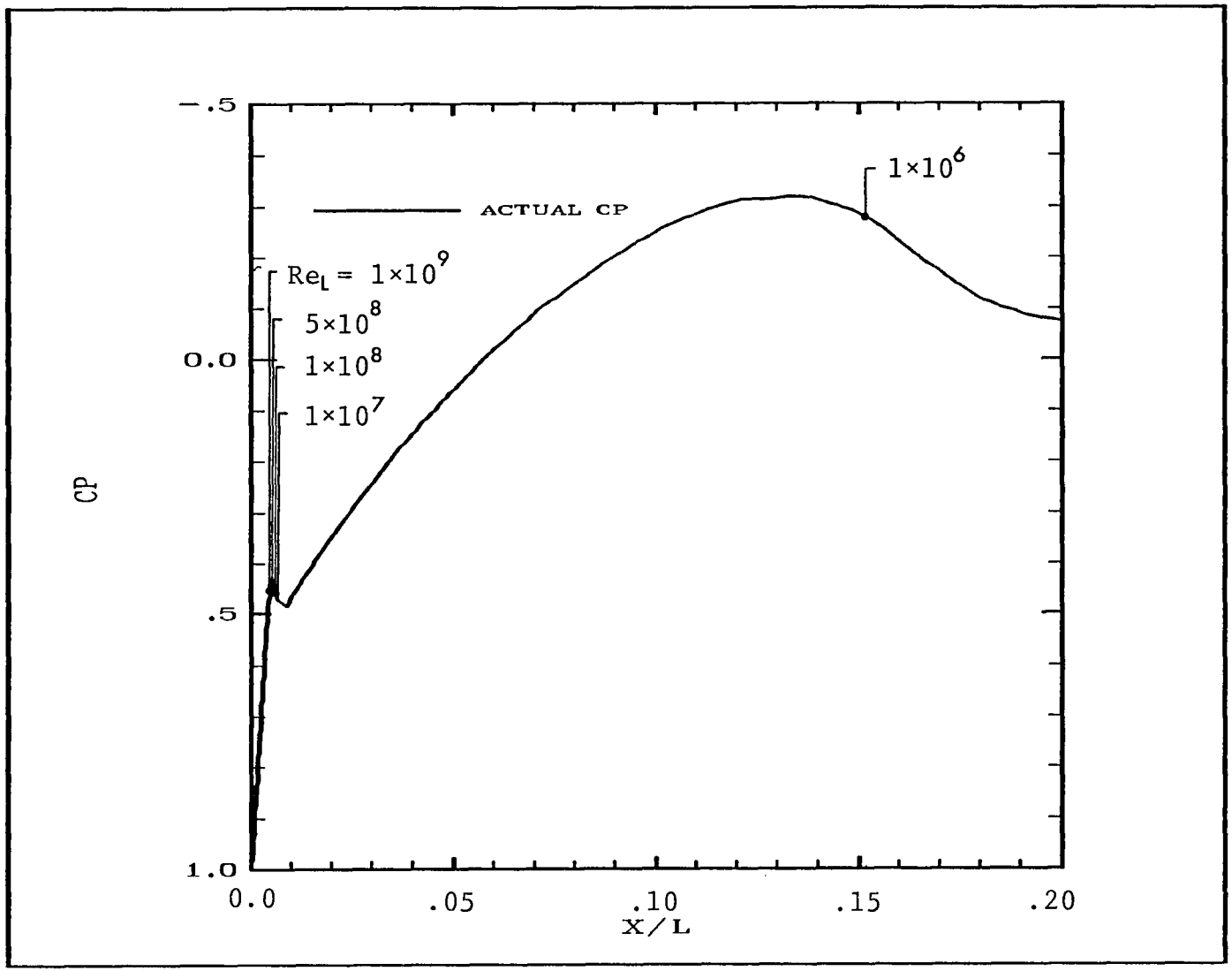

Figure 12. Neutral Stability Point as a Function of Reynolds Number for the Pathfinder I at Mach 0.6.

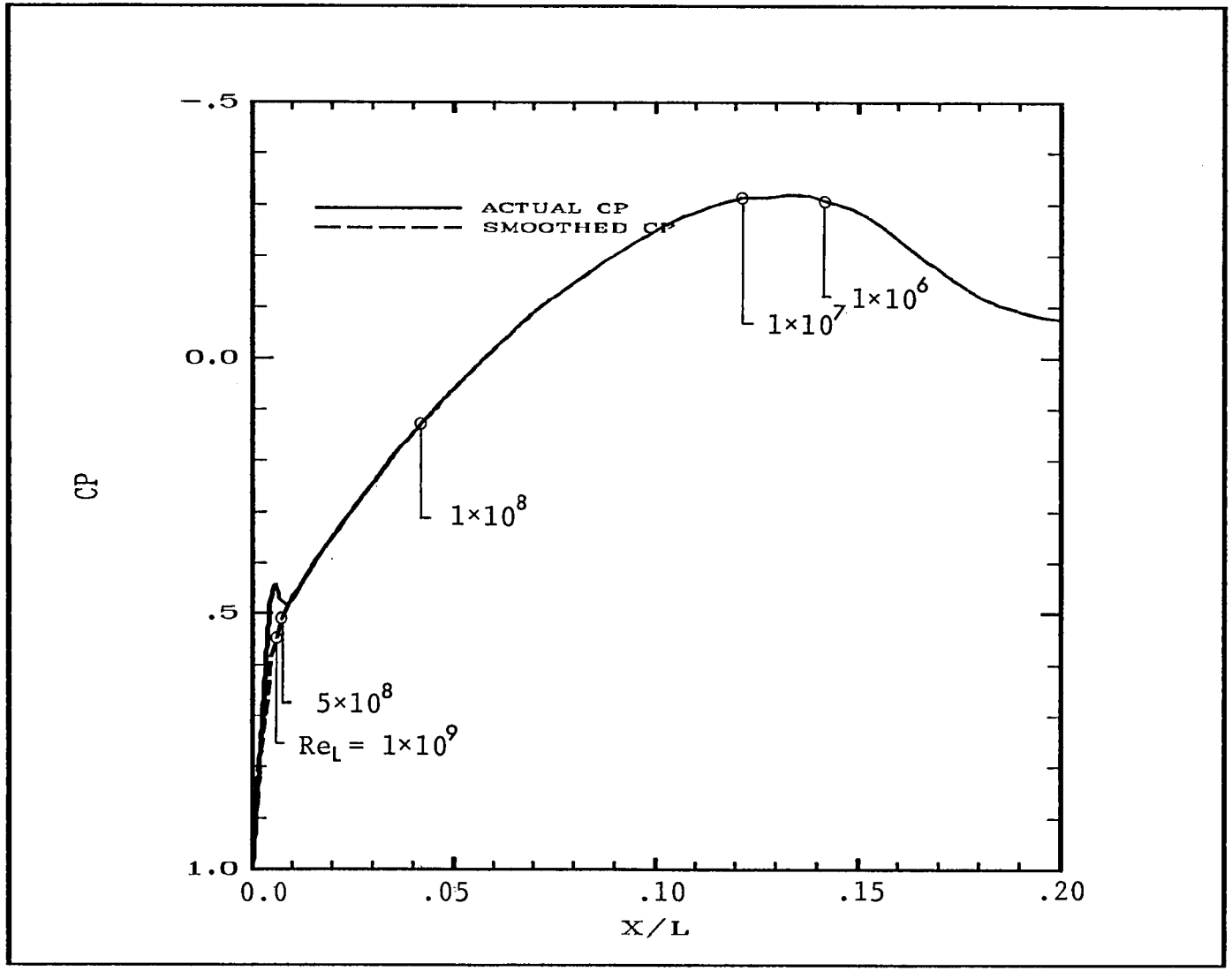

Figure 13. Neutral Stability Point as a Function of Reynolds Number for the Smoothed Pressure Distribution.

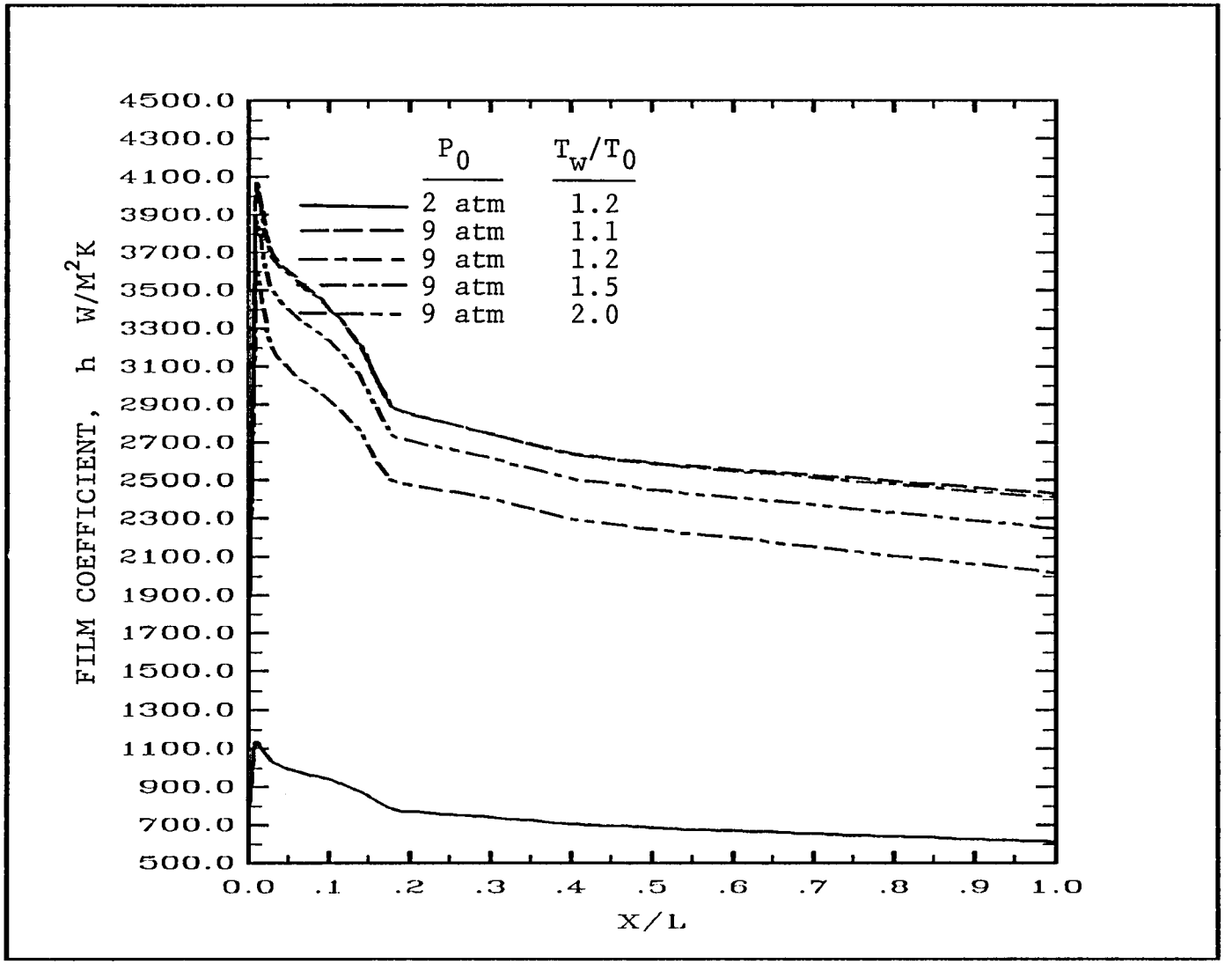

Figure 14. Heat Transfer Film Coefficient Distribution as a Function of Stagnation Pressure and Ratio of Surface-to-Stagnation Temperature at Mach 0.6.

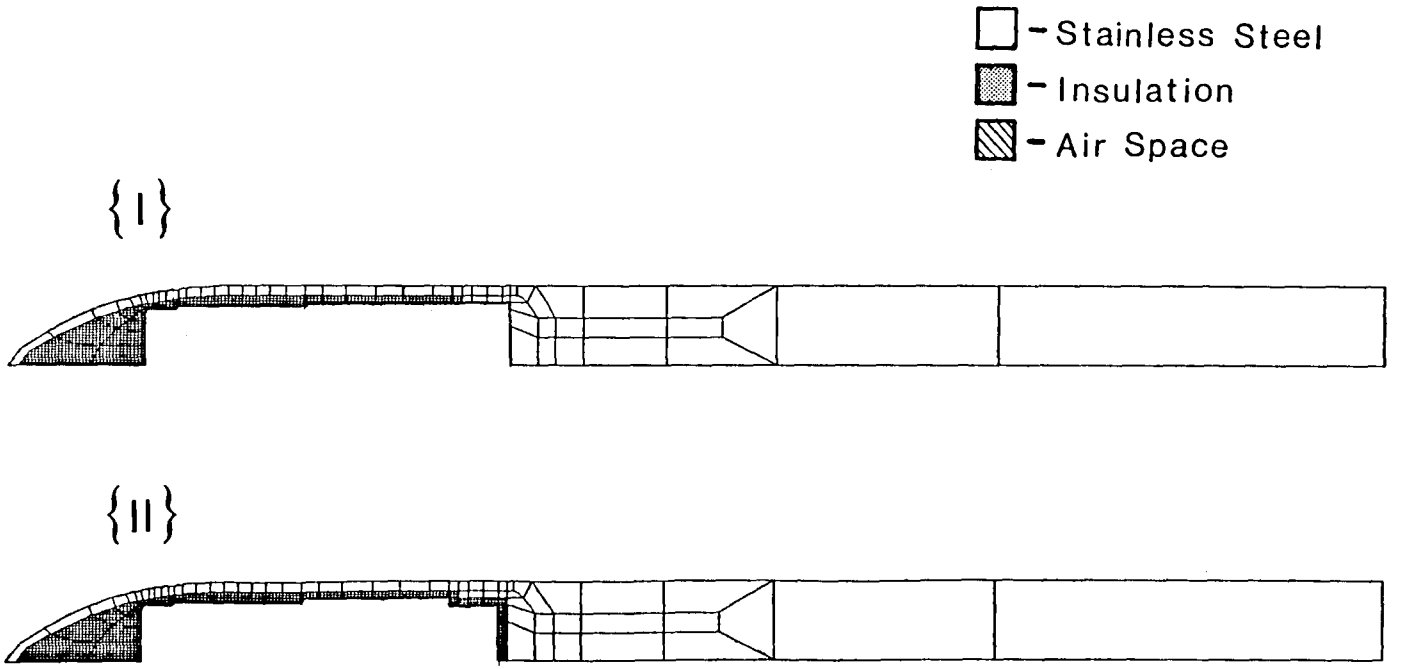

Figure 15. Configurations I, and II, used in the Thermal Analysis.

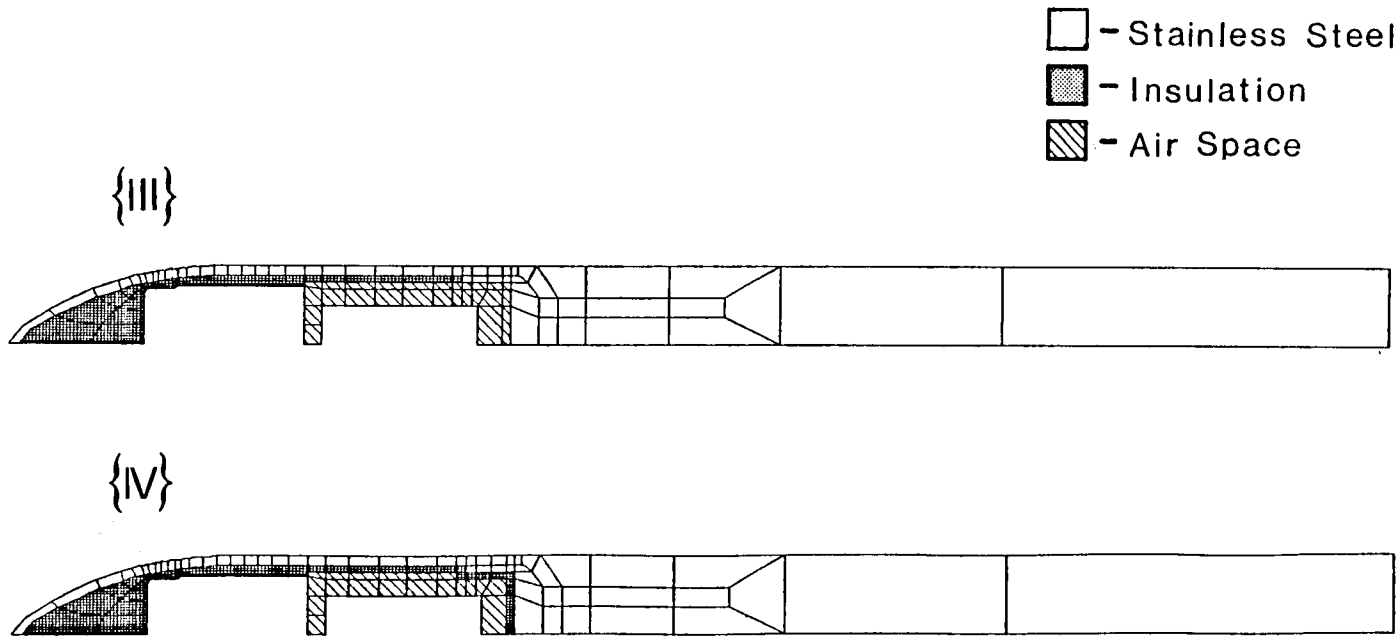

Figure 16. Configurations III, and IV, used in the Thermal Analysis.

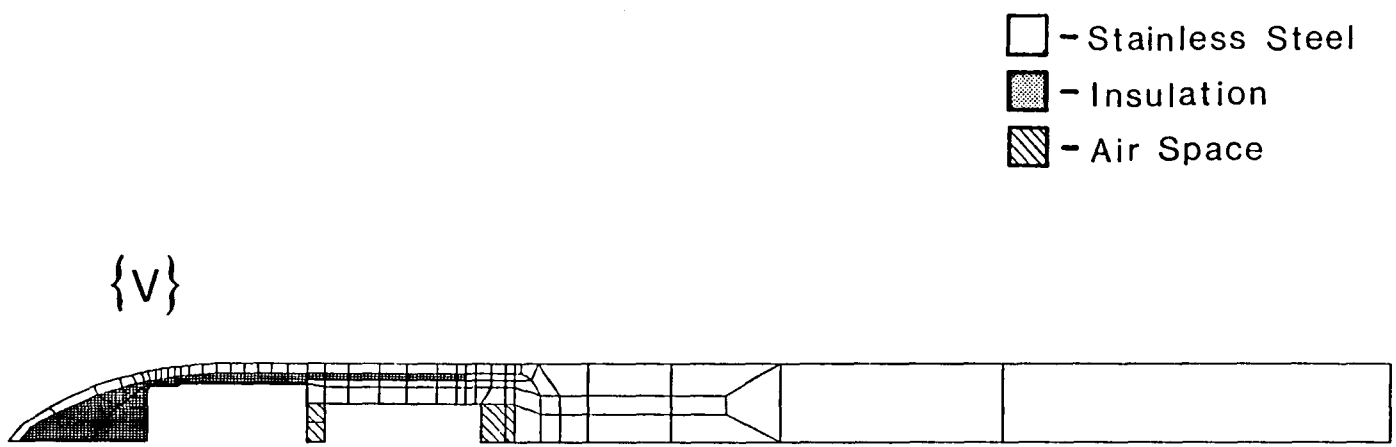

Figure 17. Configuration V used in the Thermal Analysis.

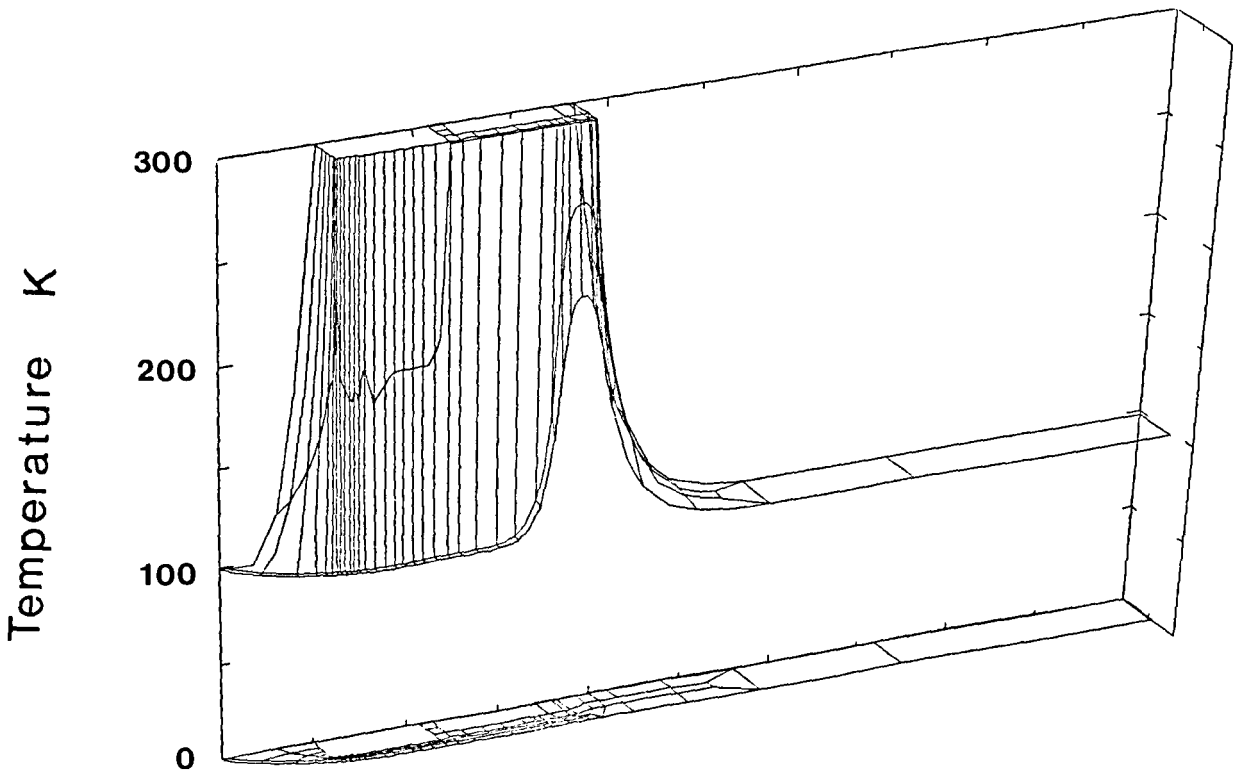

Figure 18. Body Temperature Distribution for Configuration I.

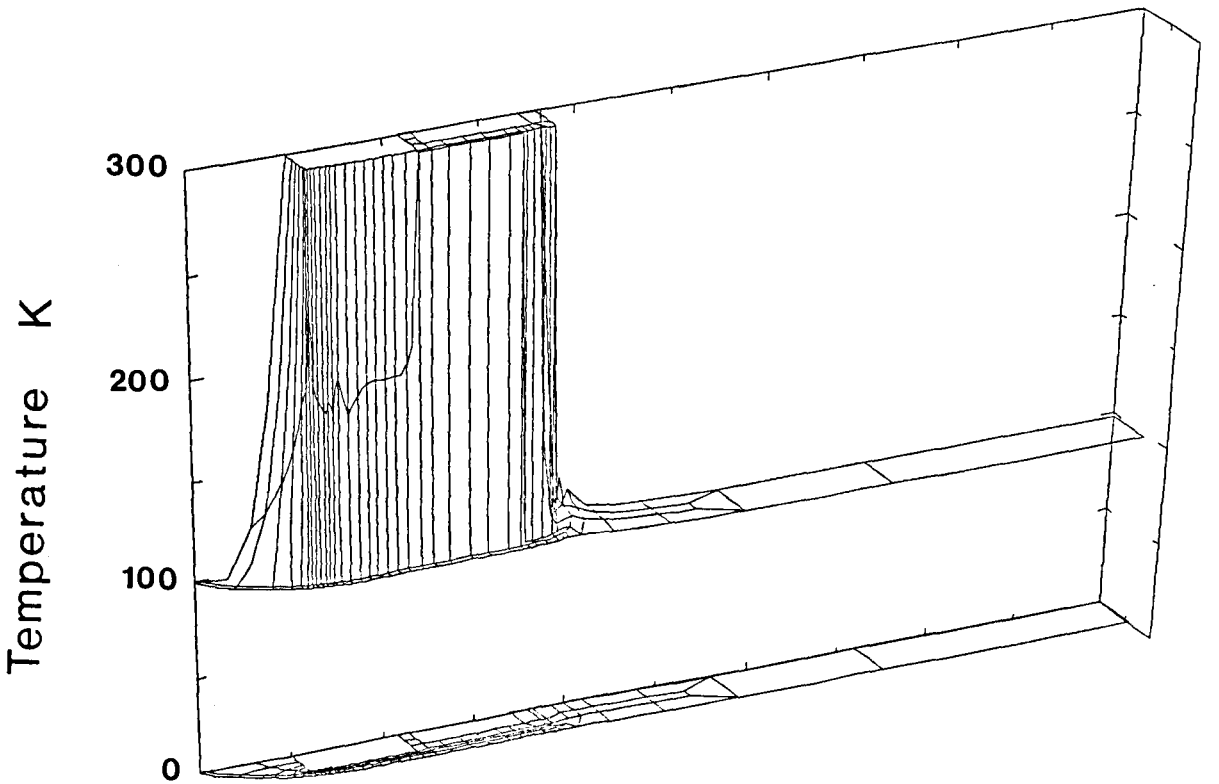

Figure 19. Body Temperature Distribution for Configuration II.

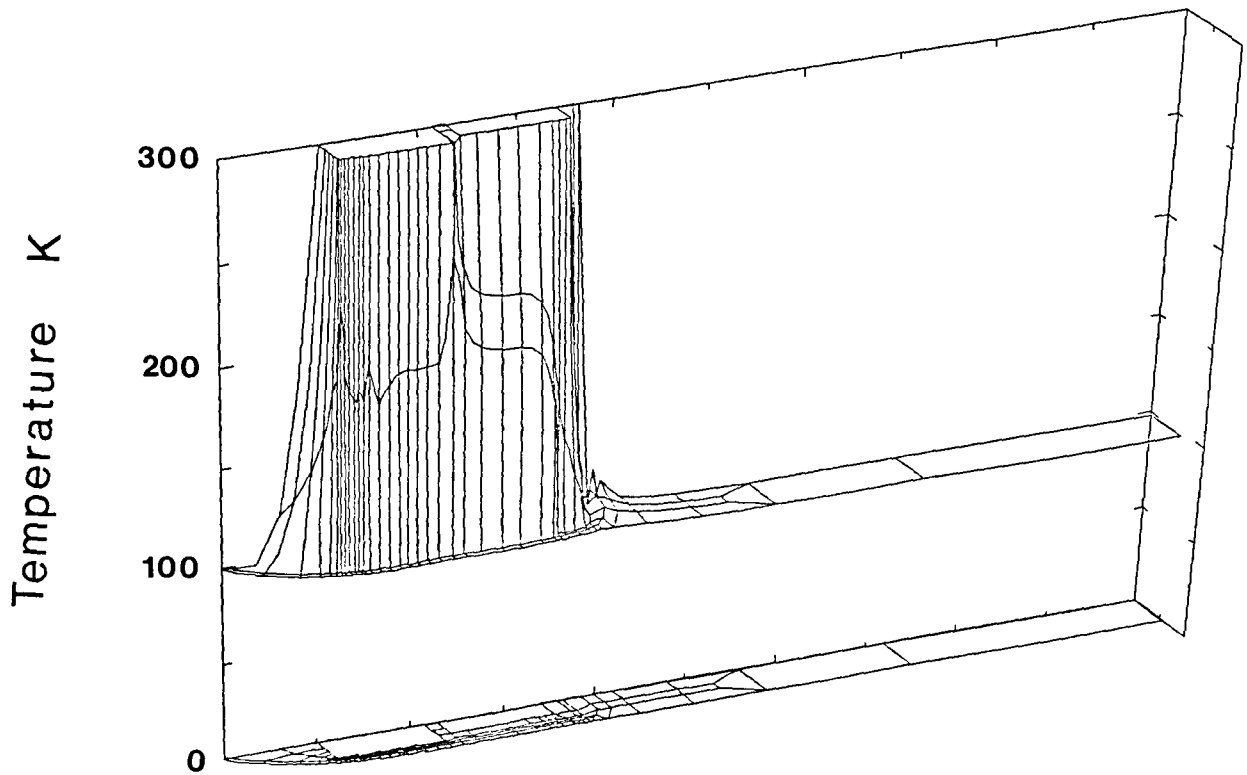

Figure 20. Body Temperature Distribution for Configuration III.

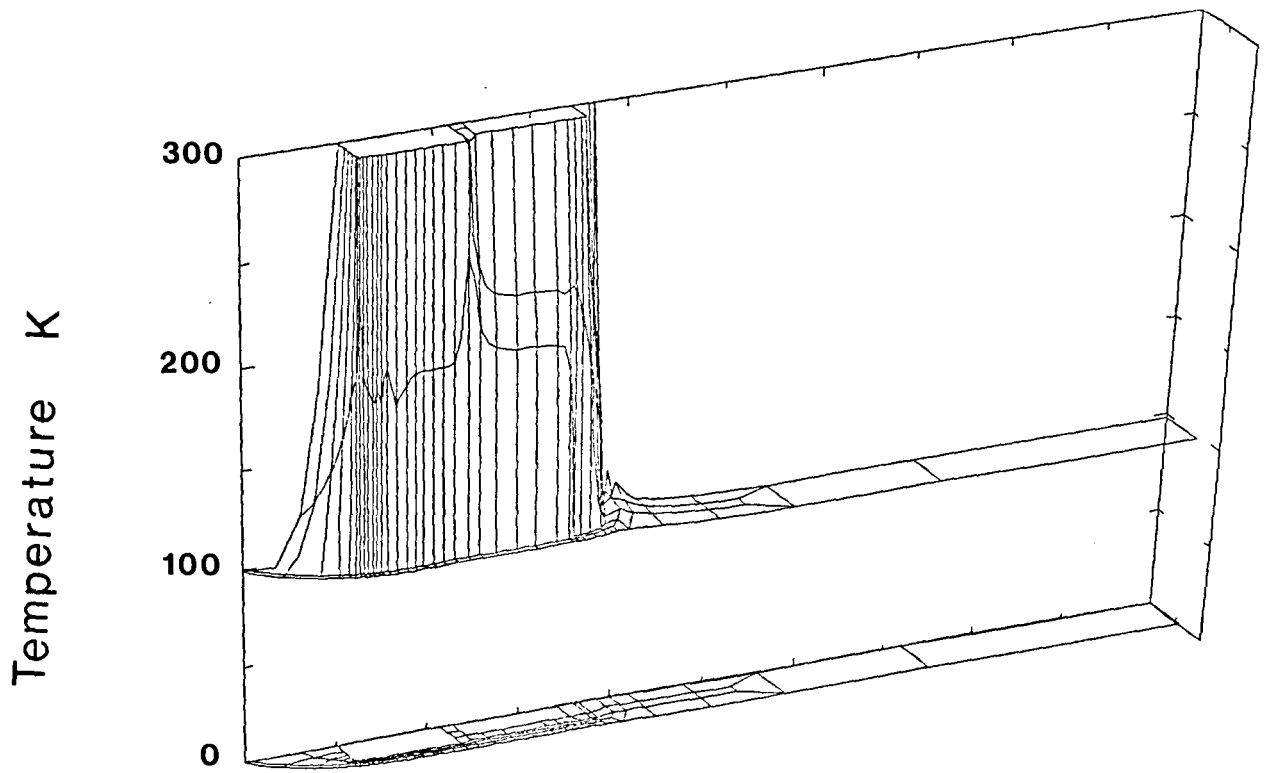

Figure 21. Body Temperature Distribution for Configuration IV.

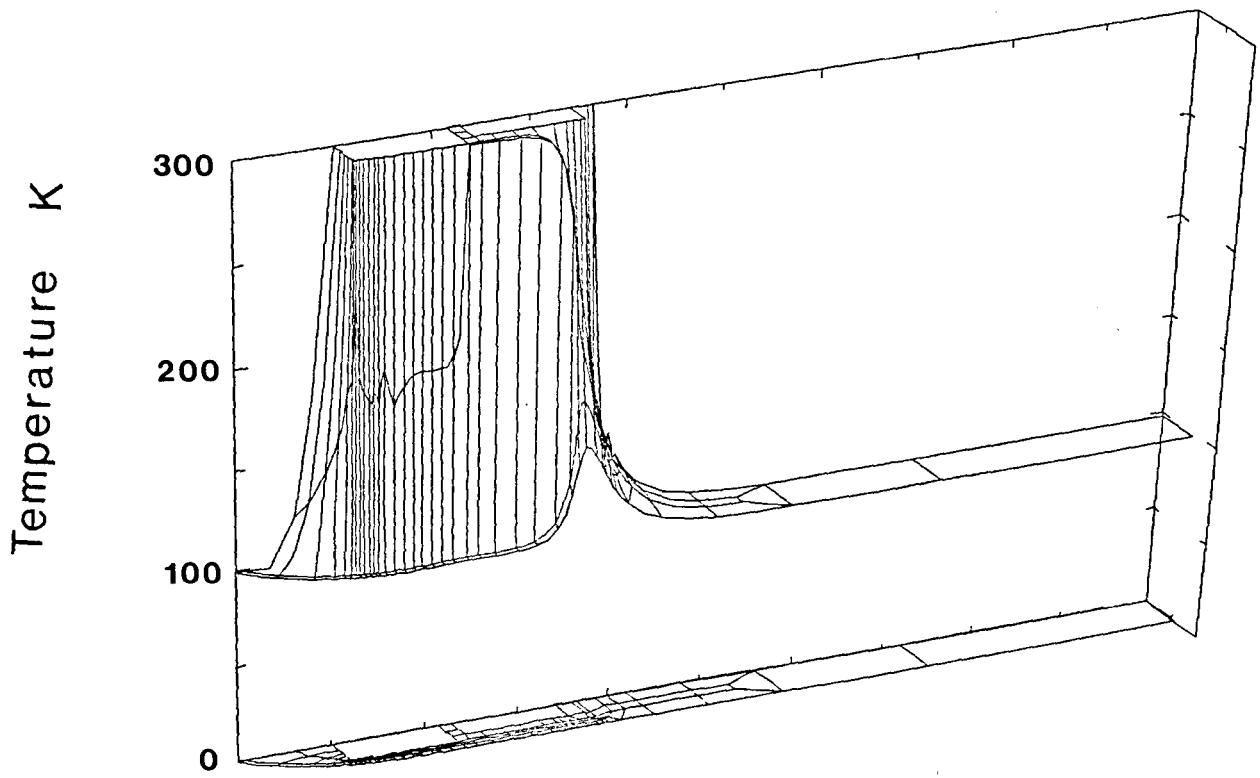

Figure 22. Body Temperature Distribution for Configuration V.

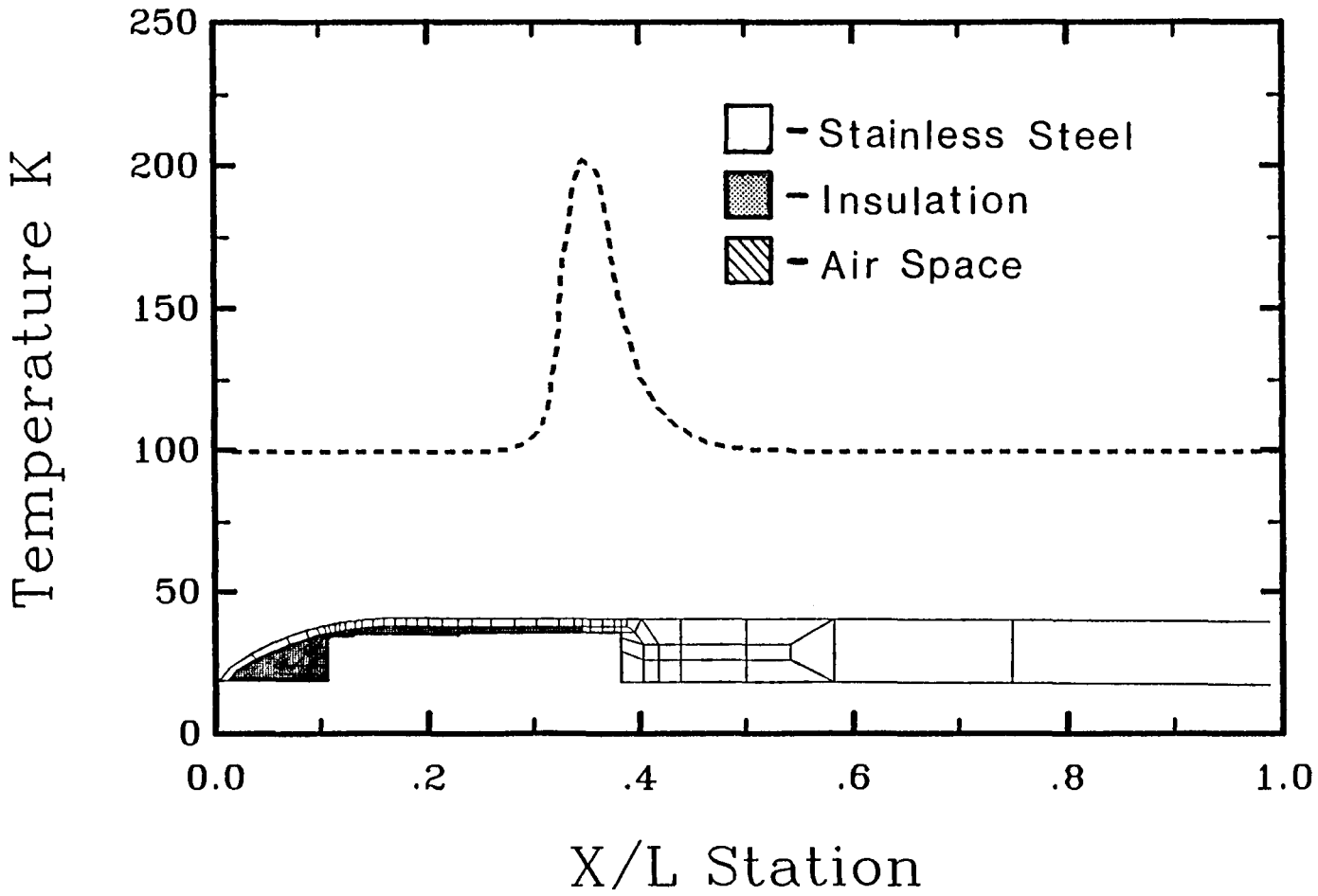

Figure 23. Surface Temperature Distribution for Configuration I, Mach 0.6, 2 atm.

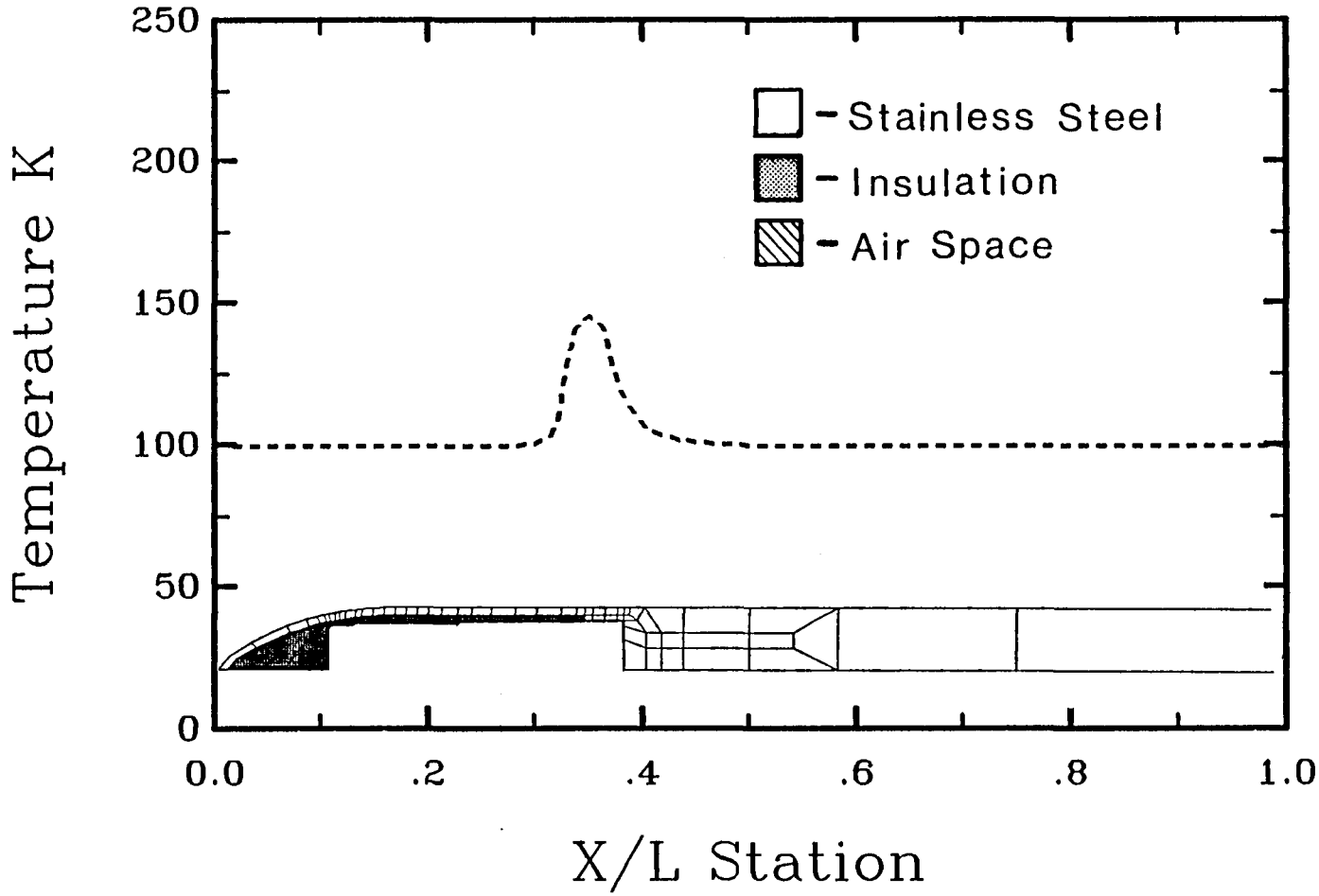

Figure 24. Surface Temperature Distribution for Configuration I, Mach 0.6, 9 atm.

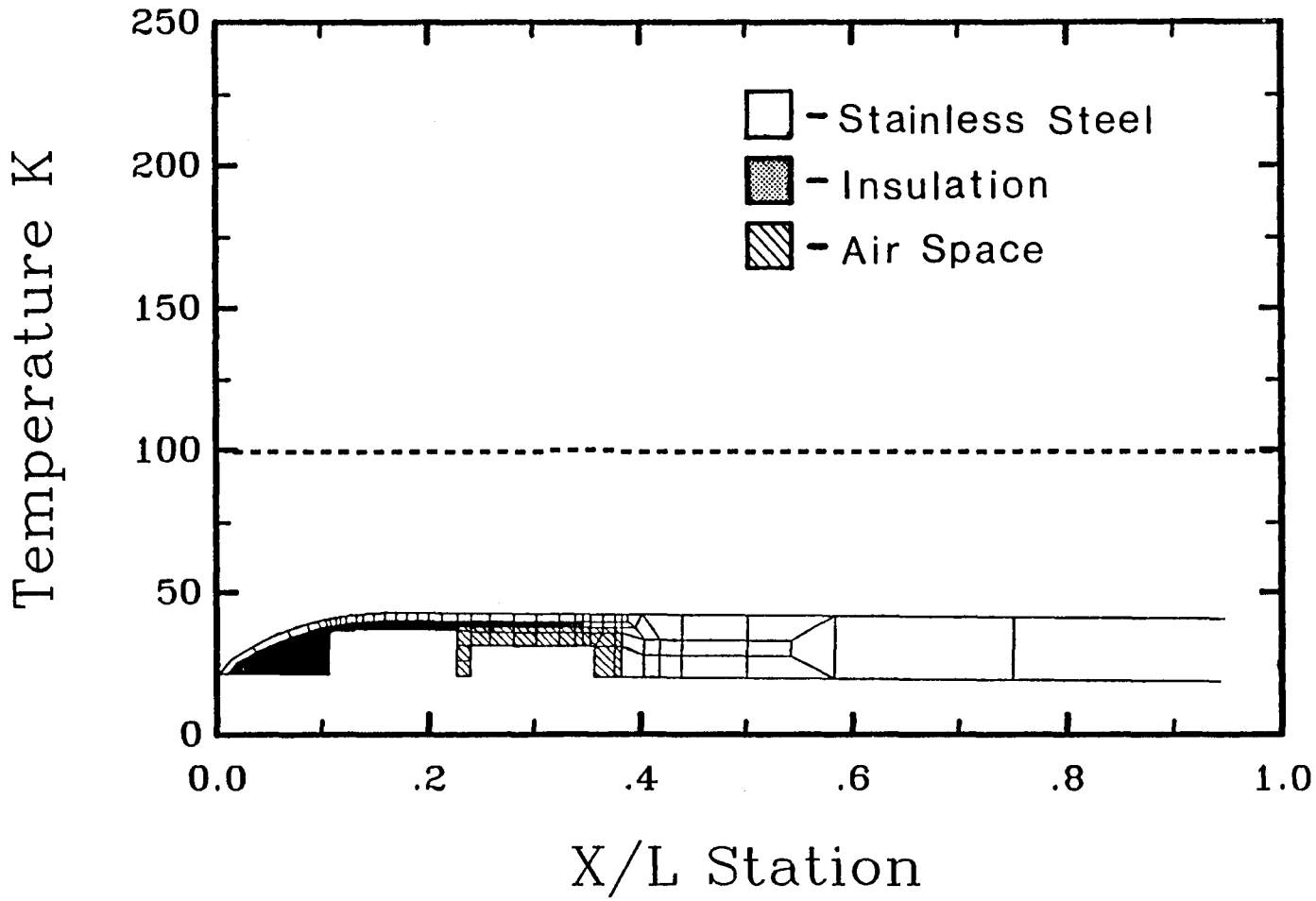

Figure 25. Surface Temperature Distribution for Configuration III, Mach 0.6, 2 atm.

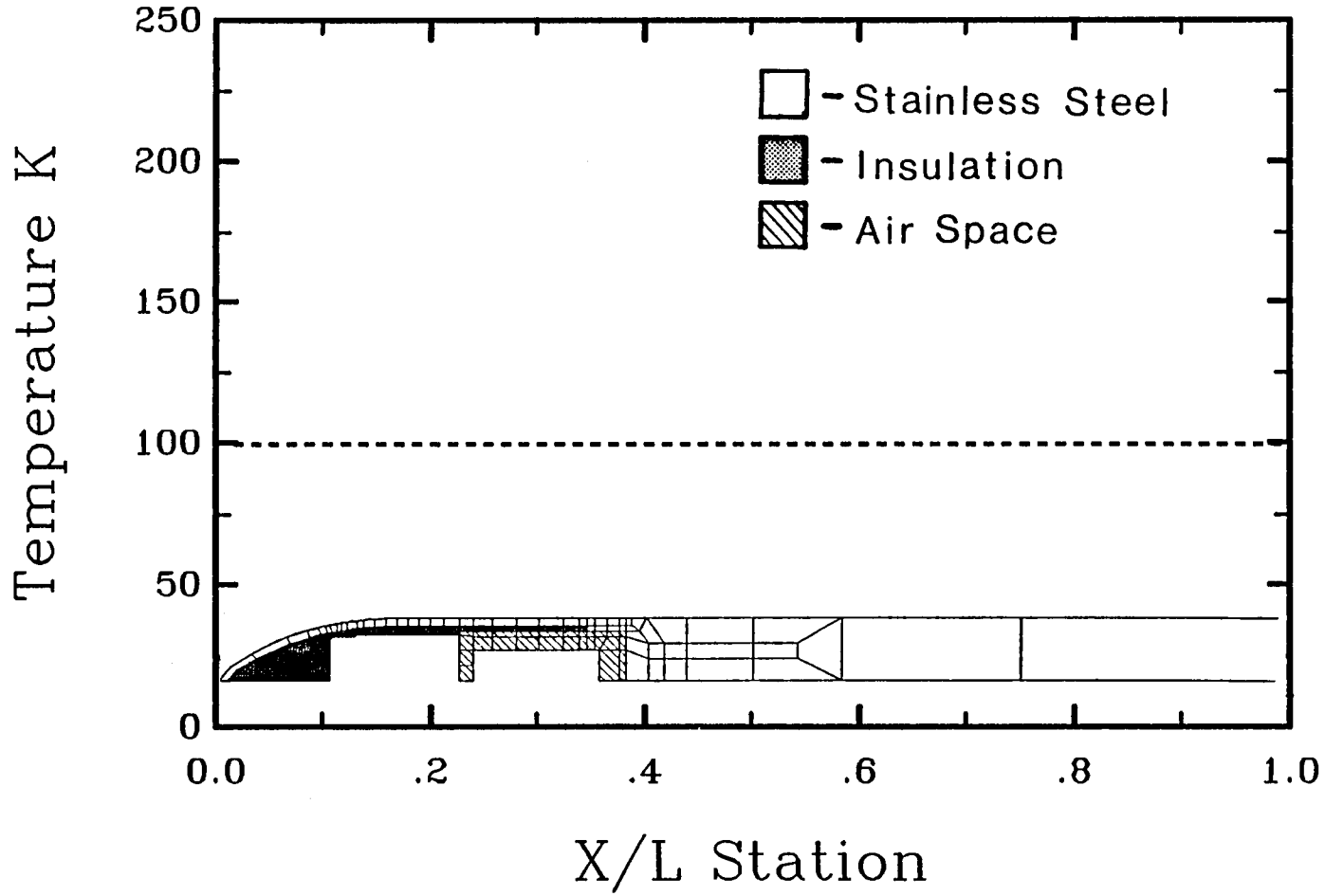

Figure 26. Surface Temperature Distribution for Configuration III, Mach 0.6, 9 atm.

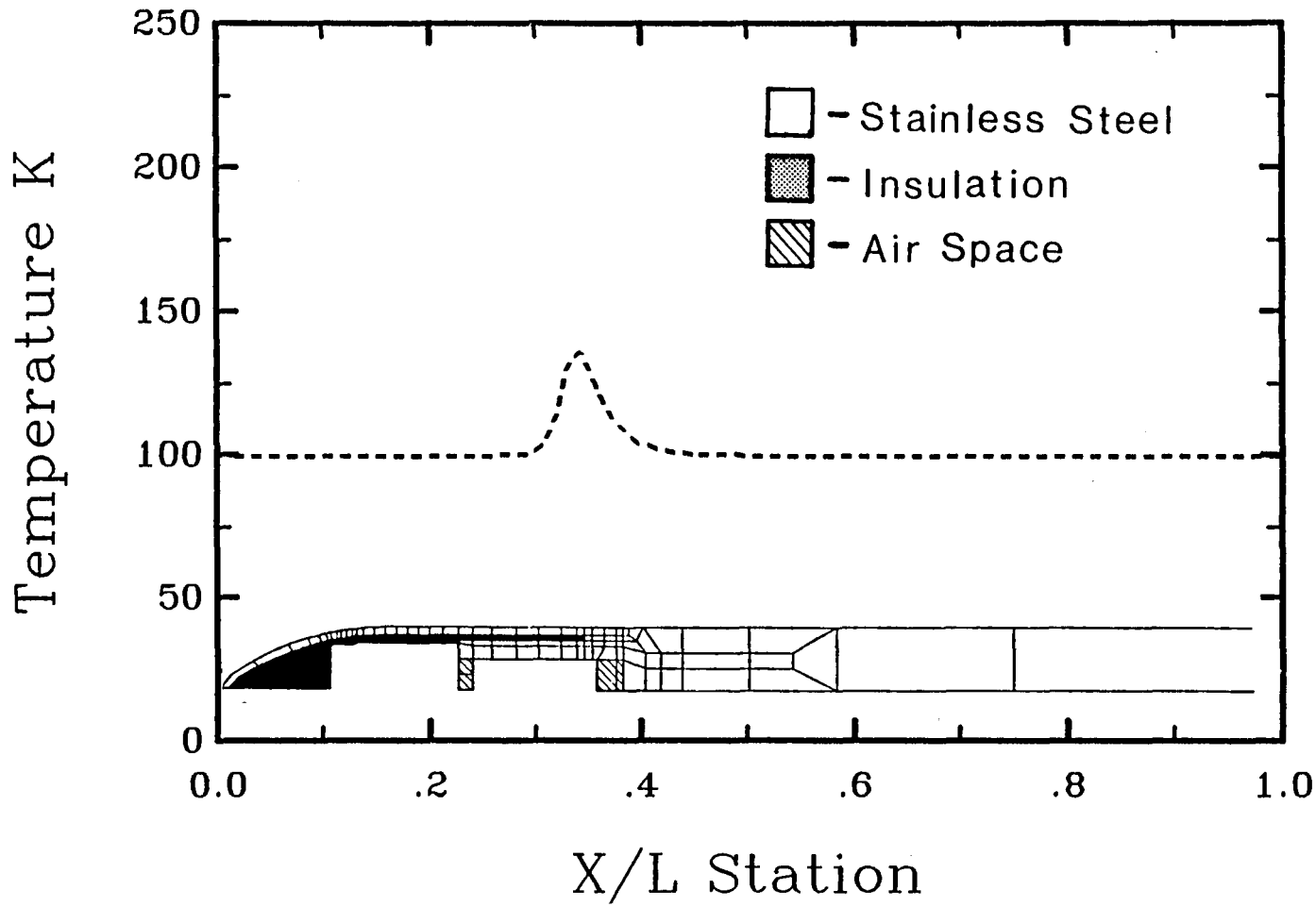

Figure 27. Surface Temperature Distribution for Configuration V, Mach 0.6, 2 atm.

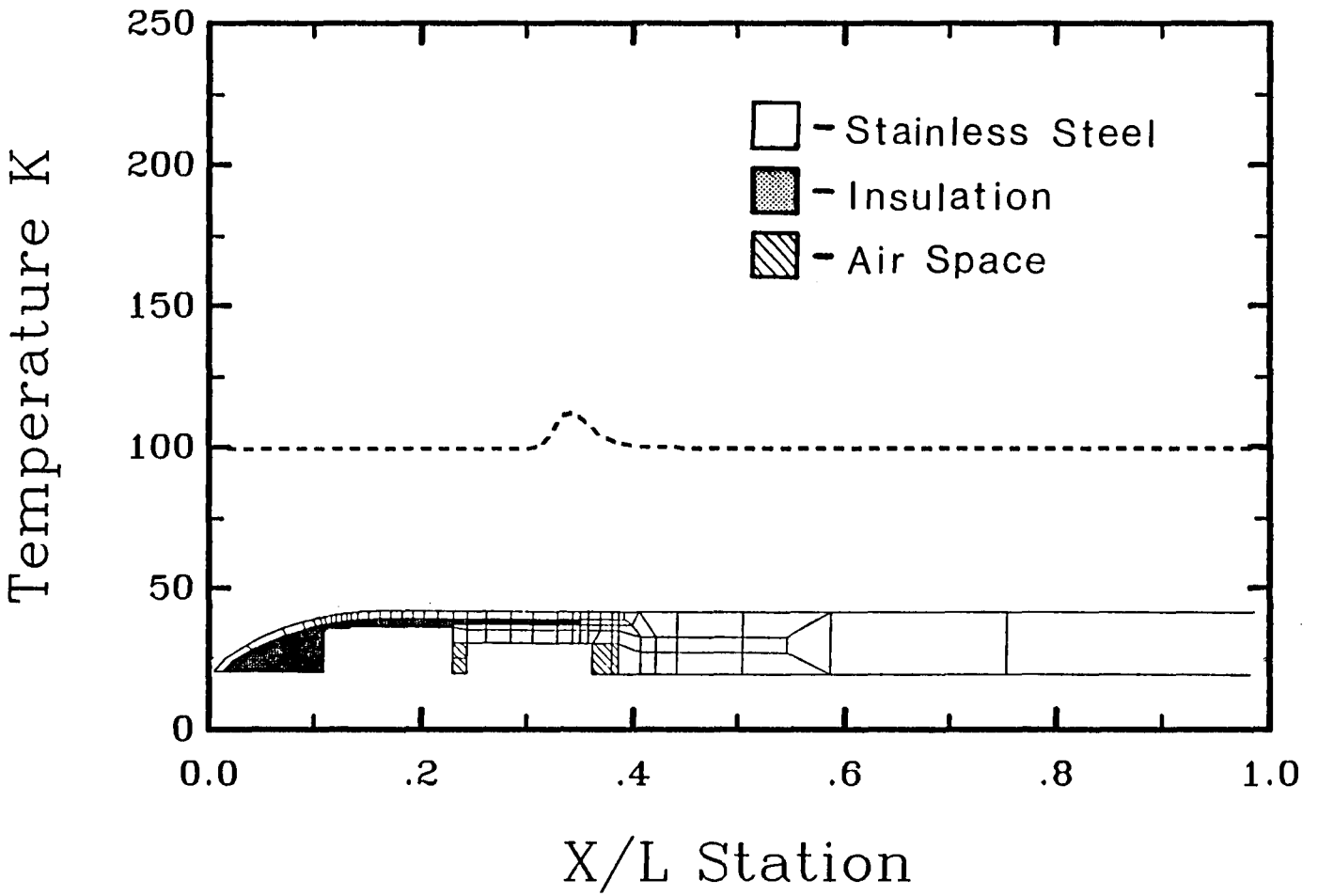

Figure 28. Surface Temperature Distribution for Configuration V, Mach 0.6, 9 atm.

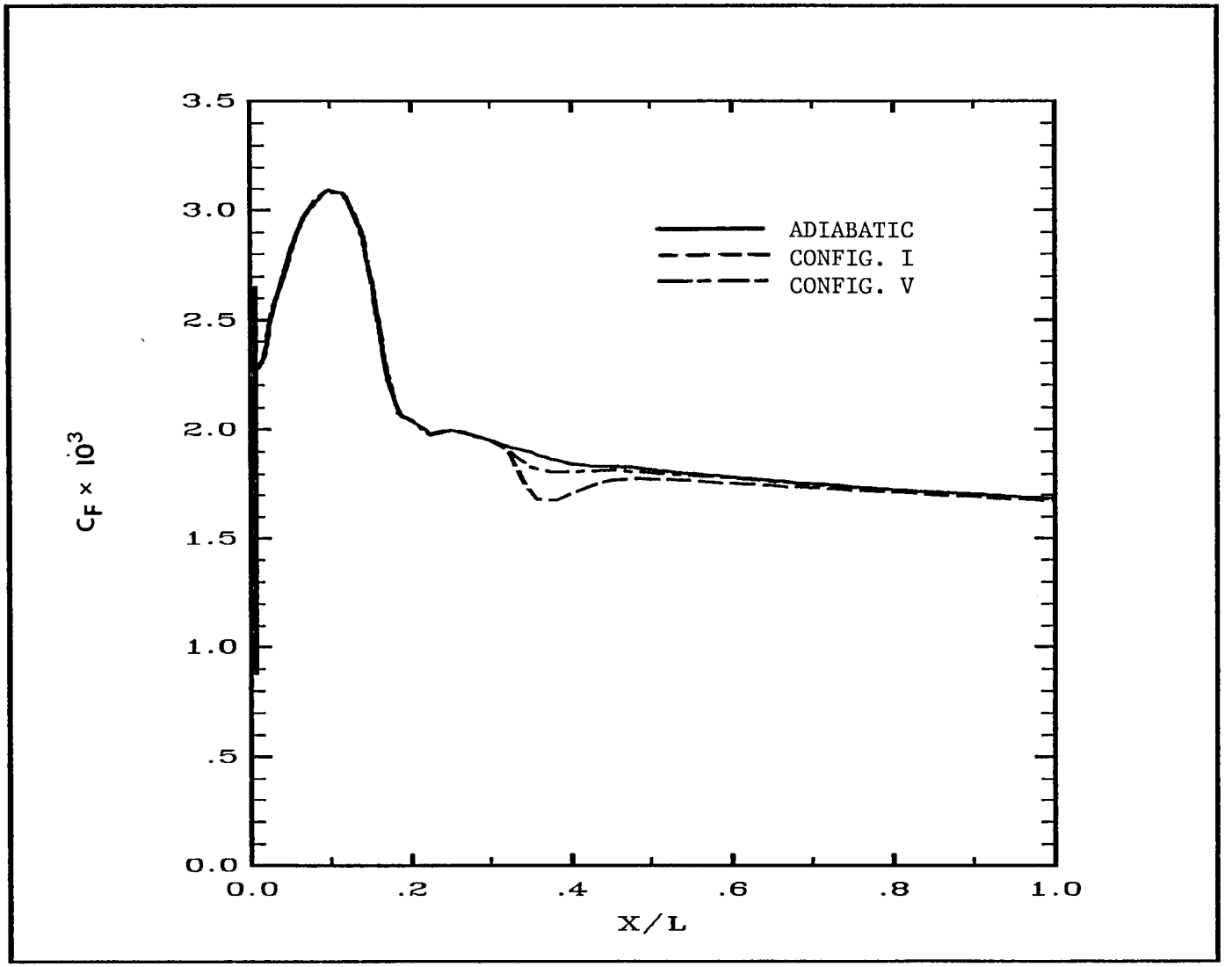

Figure 29. Skin Friction Coefficient Distributions for Configurations I and V, Mach 0.6, 2 atm.

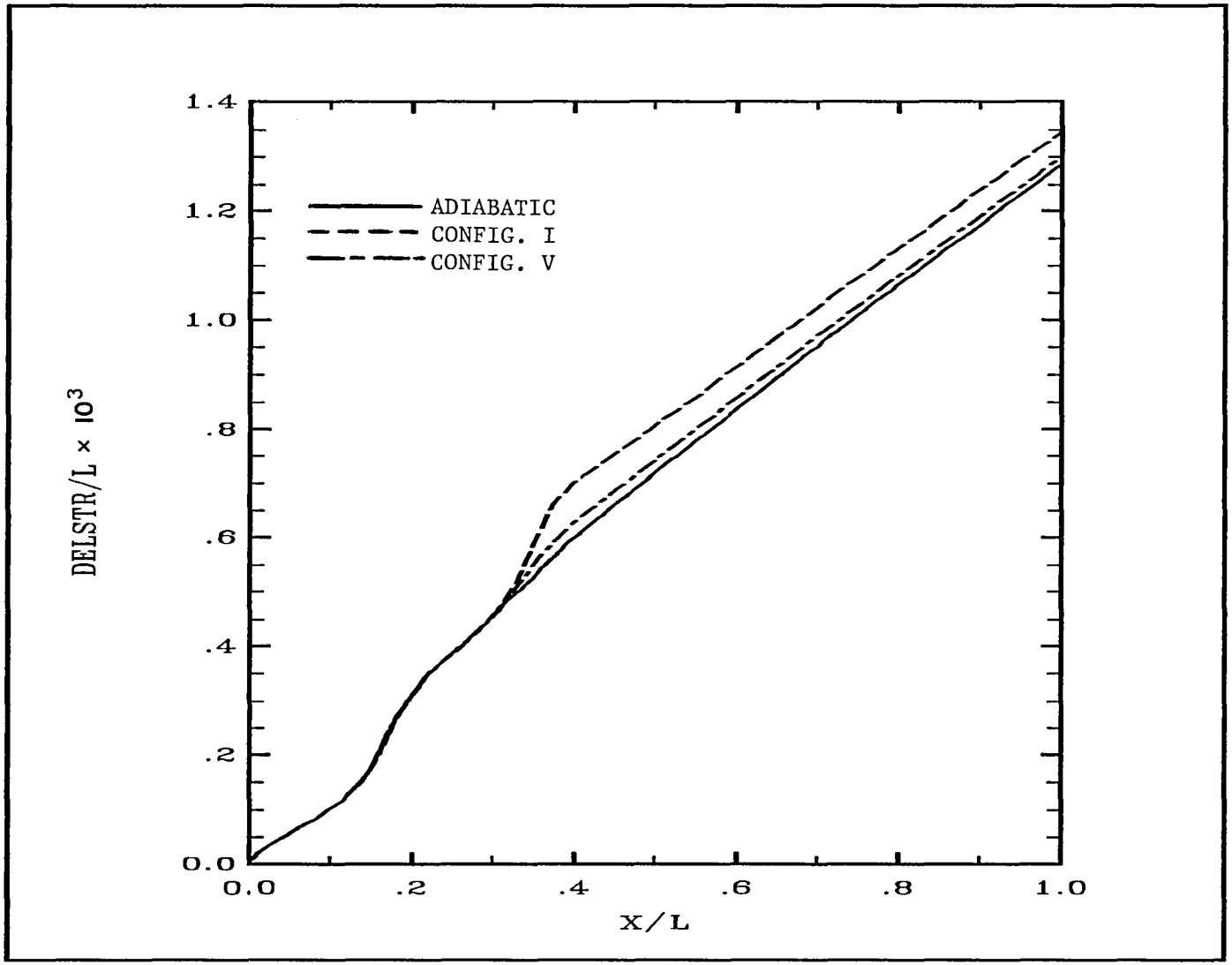

Figure 30. Boundary Layer Displacement Thickness for Configurations I and V, Mach 0.6, 2 atm.

APPENDIX

FINITE ELEMENT CHECK CASES

This appendix discusses some of the check cases used to verify the two dimensional and axi-symmetric capabilities of the finite element heat transfer code developed to perform the required thermal analysis.

These check cases were various "textbook" type heat transfer problems that could be solved by hand calculations and then compared with the solutions obtained from a finite element model of the same problem. The eight node isoparametric quad element is used for every case. Three of the check cases are described below and are illustrated in Figures A1 through A3.

Case 1 is a two dimensional wall with two material layers, with thermal conductivities of k_1 = 2 W/mK, and k_2 = 10 W/mK. The temperature on one face of the wall is a uniform 300K, and the other face is exposed to convection with h = 100 W/m^2K, and a film temperature of 100K. The wall is 0.2 m thick with each layer being 0.1 m thick.

Case 2 is a cylinder with two material layers with the same conductivities as those in Case 1. The inner surface temperature is a uniform 300K, and the Case 1 convection condition is applied to the outer surface. The interior radius is 0.1 m, the outer radius is 0.3 m, and each layer is 0.1 m thick.

Case 3 is a sphere with the same materials and boundary conditions as in Cases 1 and 2. The radial dimensions of the sphere are identical to those of the cylinder.

Finite element models were developed to represent each problem and took advantage of symmetry where possible. Two models were made for the cylinder problem, one evaluating the problem as a two dimensional cross section of the cylinder. The other uses an axi-symmetric representation of the cylinder wall. The finite element grids for the check cases are shown in Figure A4.

Each problem was evaluated by hand using the thermal resistance form for the particular geometry. Figures A5 through A7 show the computed closed form solutions and the nodal temperatures computed with the finite element code for each check case. The nodal temperatures computed with the finite element code and the corresponding temperature from the "exact" solution are virtually identical. Some slight variation is noted between the values for corner and mid-side nodes, but were typically no more than a tenth of a degree. The deviations between the exact solution and the node temperatures computed for the plane wall were identical to a few thousandths of a degree. The cylinder and the sphere cases compared

very well with the results of the hand calculations, with typical variations from a few hundredths to a few tenths of a degree. The maximum variation occurred for the spherical case and was just less than one degree, which represents an error of about 0.6 percent. It should be noted that the two dimensional model of the cylinder and the axi-symmetric model used for the sphere consisted of only eight elements, which are rather crude models of the actual geometry.

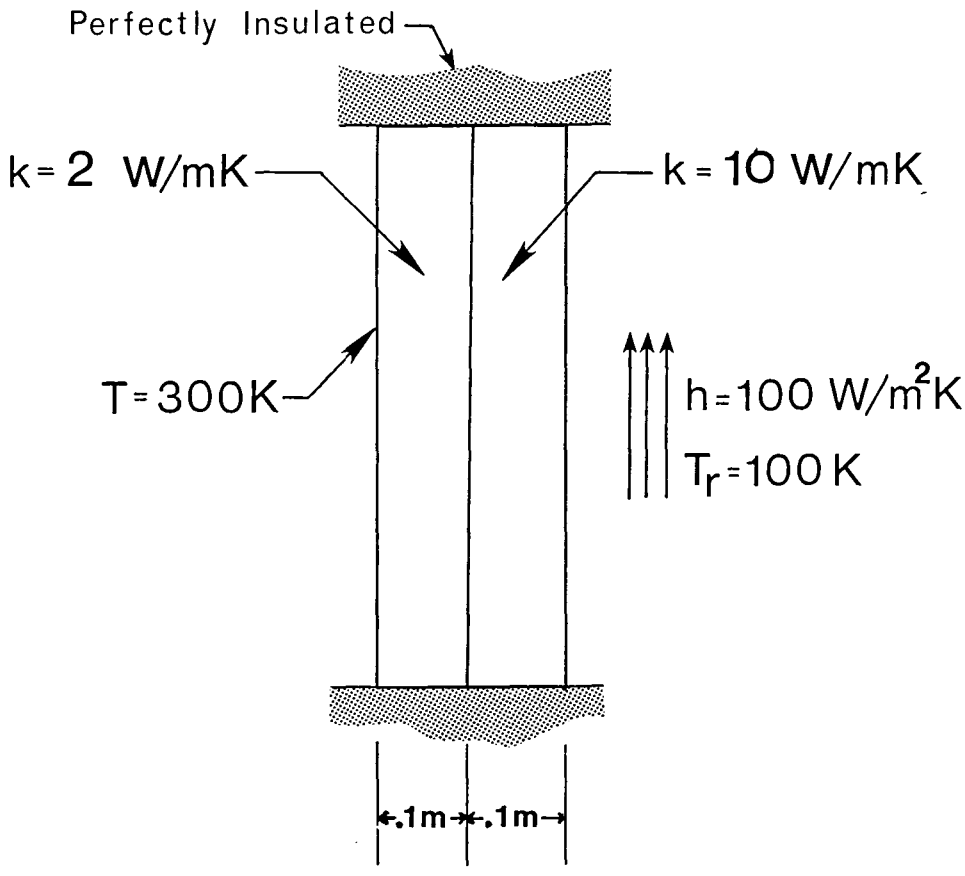

Figure A1. Plane Wall Check Case.

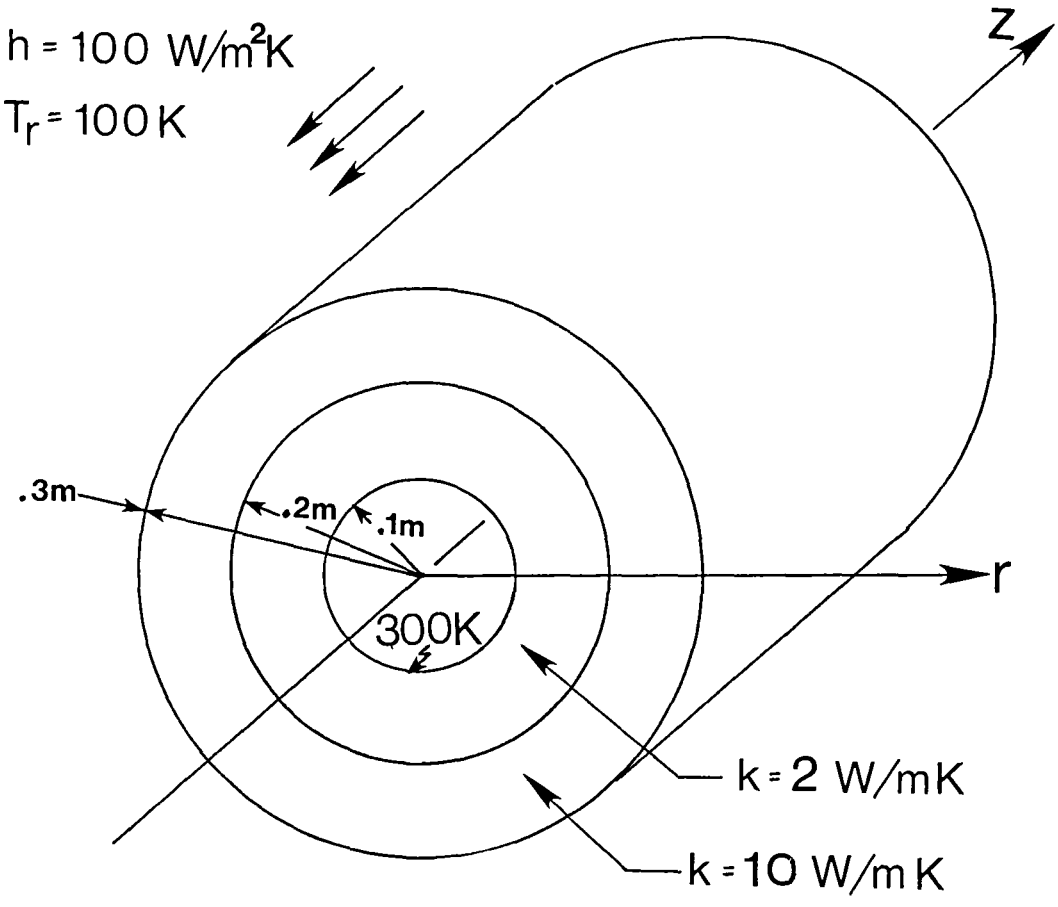

Figure A2. Cylindrical Check Case.

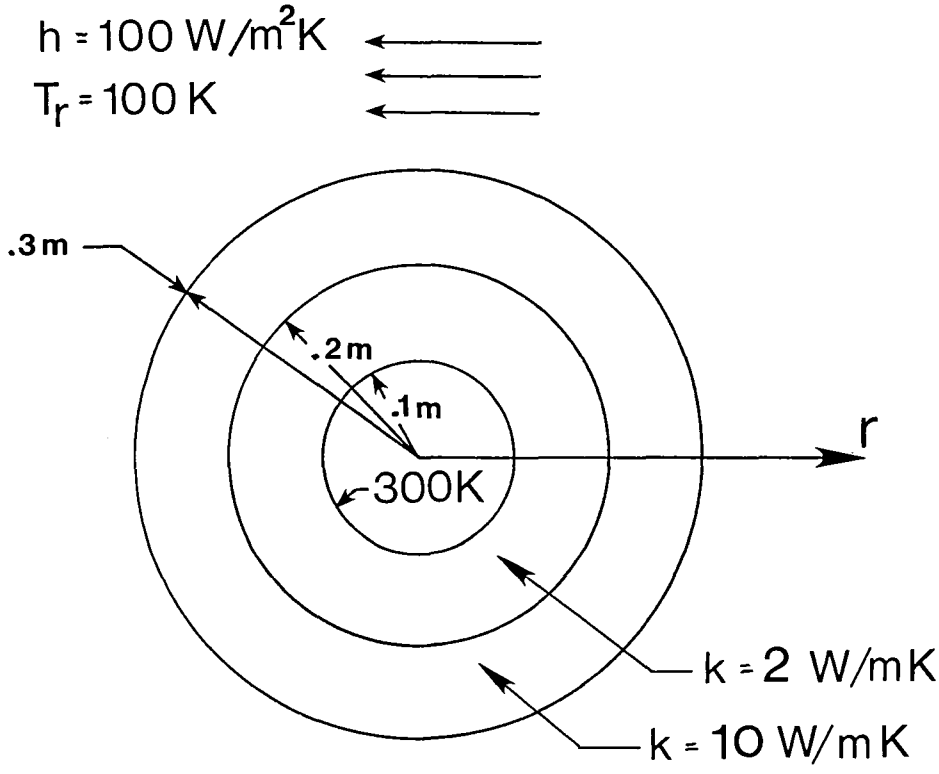

Figure A3. Spherical Check Case.

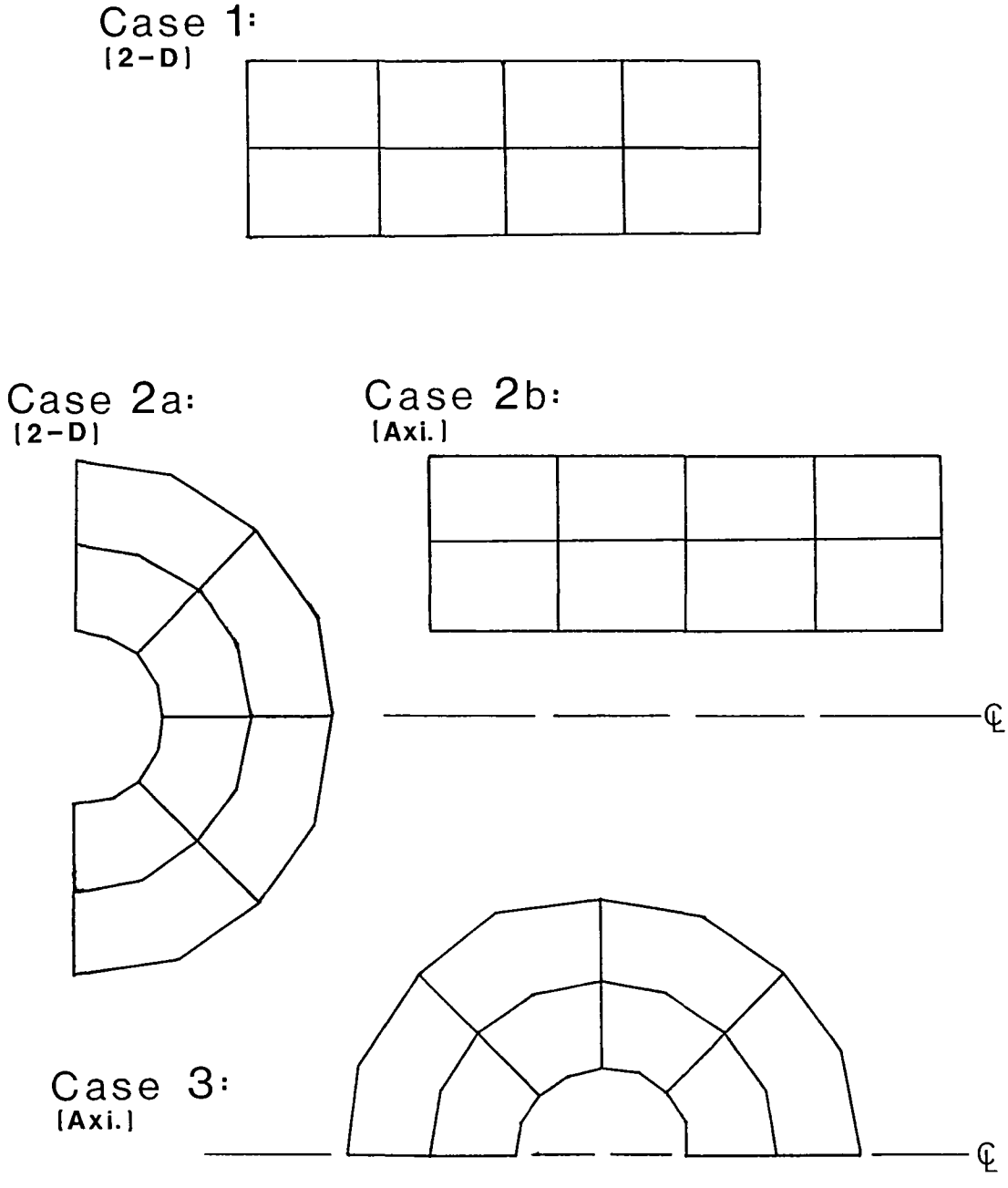

Figure A4. Check Case Finite Element Grids.

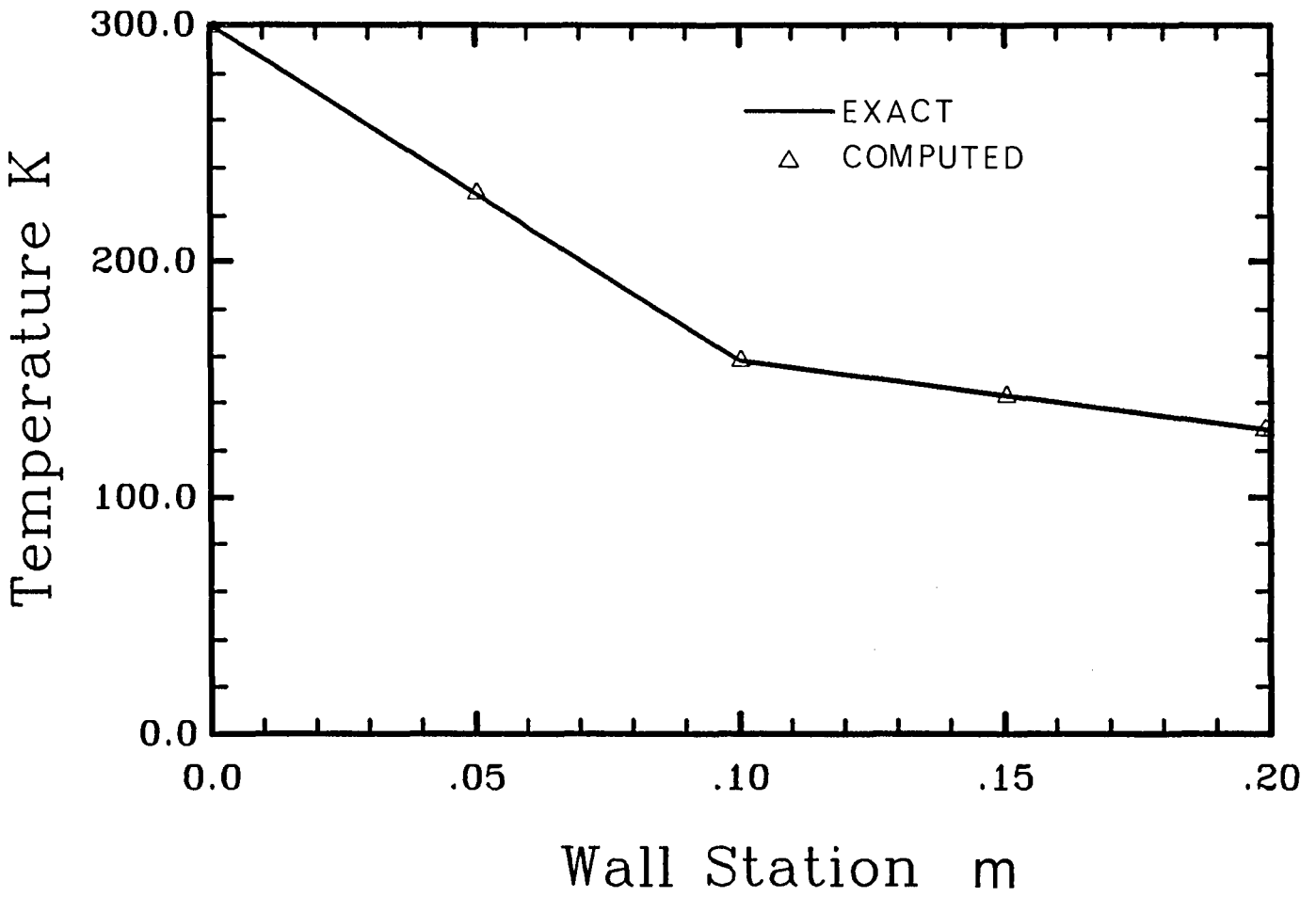

Figure A5. Nodal and Exact Temperatures, Case I.

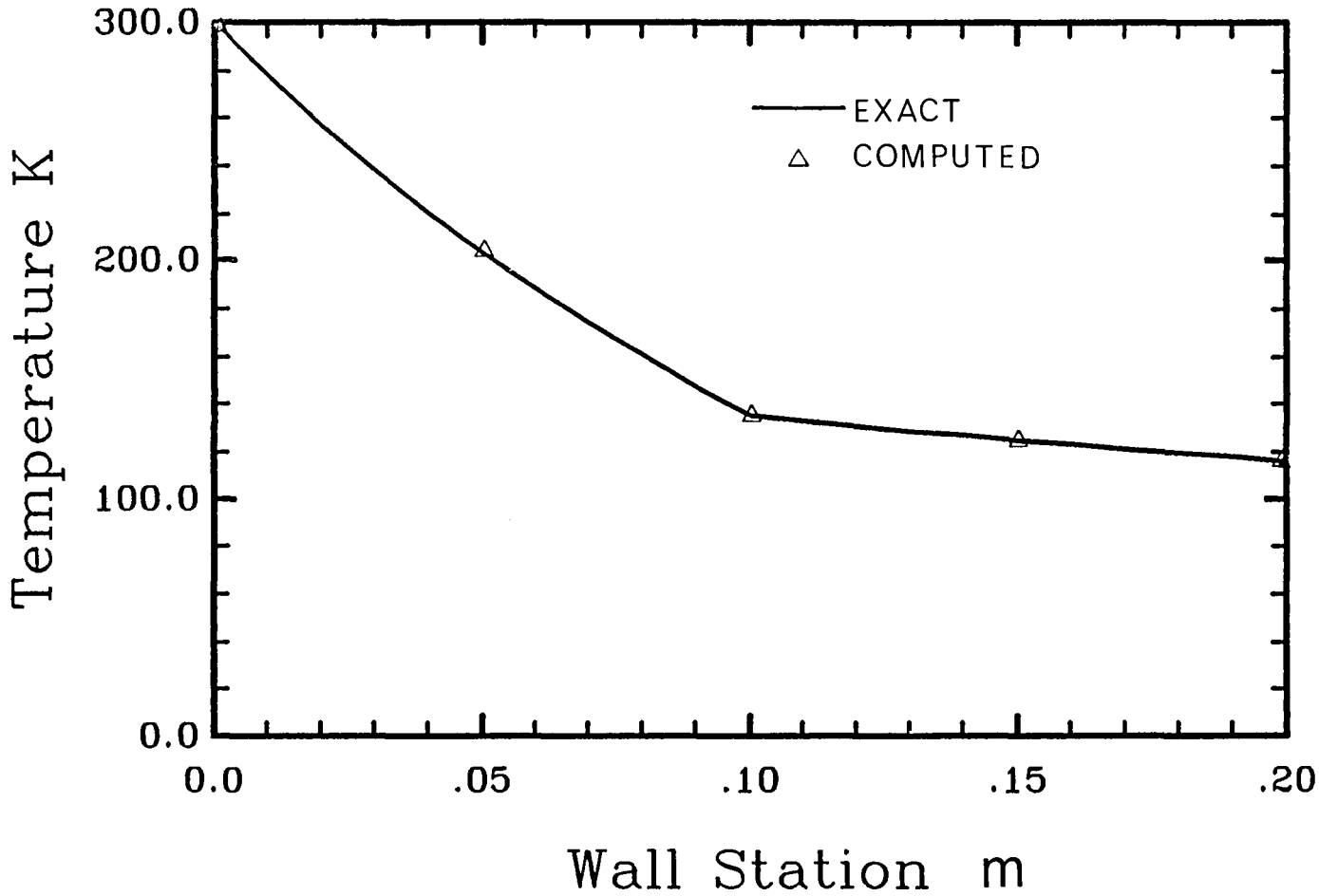

Figure A6. Nodal and Exact Temperatures, Case 2.

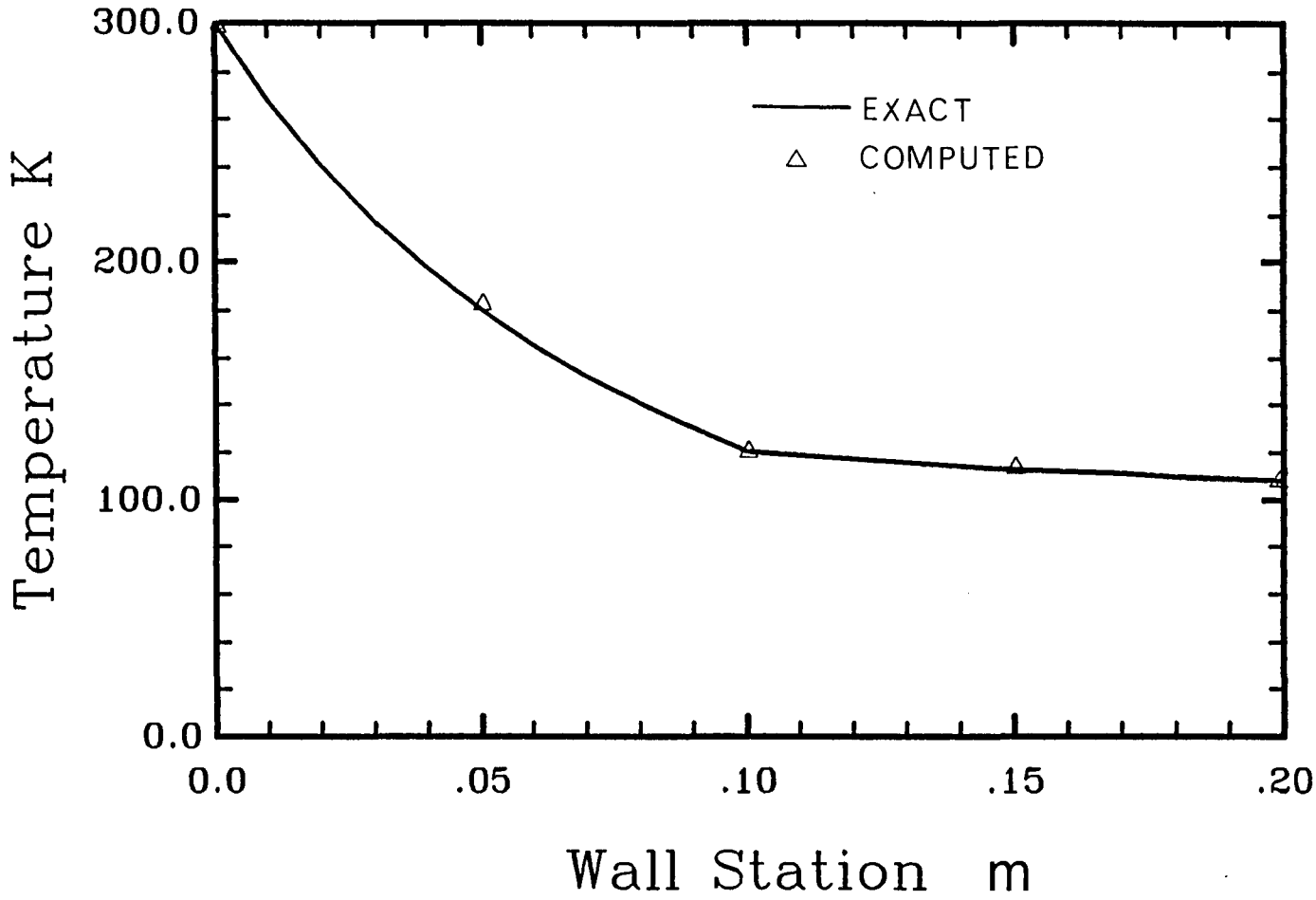

Figure A7. Nodal and Exact Temperatures, Case 3.

1. Report No.	2. Government Accession No.	3. Recipient's Catalog No.
NASA CR-3924		

4. Title and Subtitle	5. Report Date
A Theoretical Study of Non-Adiabatic Surface Effects for a Model in the NTF Cryogenic Wind Tunnel	August 1985
	6. Performing Organization Code
7. Author(s)	8. Performing Organization Report No.
J. M. Macha, L. A. Pare, and D. B. Landrum	TR 83-4975-02
	10. Work Unit No.
9. Performing Organization Name and Address	
Texas A&M Research Foundation College Station, Texas 77843	11. Contract or Grant No. NAG1-417
	13. Type of Report and Period Covered Contractor Report 10-1-83 1-31-85
12. Sponsoring Agency Name and Address	
National Aeronautics and Space Administration Washington, DC 20546	14. Sponsoring Agency Code 505-31-53-10

15. Supplementary Notes

Langley Technical Monitor: Charles B. Johnson
Principal Investigator: J. Michael Macha

16. Abstract

A theoretical analysis has been made of the severity and effect of non-adiabatic surface conditions for a model in the NTF cryogenic wind tunnel. The non-adiabatic condition arises from heaters that are used to maintain a constant thermal environment for instrumentation internal to the model. The analysis was made for several axi-symmetric representations of a fuselage cavity, using a finite-element heat conduction code. Potential flow and boundary layer codes were used to calculate the convection boundary condition for the exterior surface of the model. The results of the steady-state analysis show that it is possible to maintain the surface temperature very near the adiabatic value, with the judicious use of insulating material. Even for the most severe non-adiabatic condition studied, the effects on skin friction drag and displacement thickness were only marginally significant. The thermal analysis also provided an estimate of the power required to maintain a specified cavity temperature.

17. Key Words (Suggested by Author(s))	18. Distribution Statement
Cryogenic Wind Tunnels Model Design Boundary Layers Non-Adiabatic Surface Effects	Unclassified - Unlimited Subject Category 34

19. Security Classif. (of this report)	20. Security Classif. (of this page)	21. No. of Pages	22. Price
Unclassified	Unclassified	58	A04

For sale by the National Technical Information Service, Springfield, Virginia 22161

NASA-Langley, 1985

End of Document